Sorting of secretory proteins at the trans-Golgi network by human TGN46

Pablo Lujan[1], Carla Garcia-Cabau[2,#], Yuichi Wakana[3,#], Javier Vera Lillo[1], Carmen Rodilla-Ramírez[1], Hideaki Sugiura[3], Vivek Malhotra[4,5,6], Xavier Salvatella[2,6], Maria F. Garcia-Parajo[1,6], and Felix Campelo[1,*]

[1] ICFO-Institut de Ciencies Fotoniques, The Barcelona Institute of Science and Technology, 08860, Castelldefels (Barcelona), Spain.

[2] Institute for Research in Biomedicine (IRB Barcelona), The Barcelona Institute of Science and Technology, Baldiri Reixac 10, 08028, Barcelona, Spain.

[3] School of Life Sciences, Tokyo University of Pharmacy and Life Sciences, Hachioji, Tokyo 192-0392, Japan.

[4] Centre for Genomic Regulation (CRG), The Barcelona Institute of Science and Technology, Barcelona, Spain.

[5] Universitat Pompeu Fabra (UPF), Barcelona, Spain.

[6] Institució Catalana de Recerca i Estudis Avançats (ICREA), Passeig Lluís Companys 23, 08010, Barcelona, Spain.

[#] These authors contributed equally

[*] **Correspondence:**

Felix Campelo

ICFO-Institut de Ciencies Fotòniques

Av. Carl Friedrich Gauss, 3. 08860 Castelldefels, Barcelona - SPAIN

Phone: + 34 93 554 2225

e-mail: felix.campelo@icfo.eu

ABSTRACT

Secretory proteins are sorted at the trans-Golgi network (TGN) for export into specific transport carriers. However, the molecular players involved in this fundamental process remain largely elusive. Here, we identified the human transmembrane protein TGN46 as a receptor for the export of secretory cargo protein PAUF in CARTS – a class of protein kinase D-dependent TGN-to-plasma membrane carriers. We show that TGN46 is necessary for cargo sorting and loading into nascent carriers at the TGN. By combining quantitative fluorescence microscopy and mutagenesis approaches, we further discovered that the lumenal domain of TGN46 encodes for its cargo sorting function. In summary, our results define a cellular function of TGN46 in sorting secretory proteins for export from the TGN.

KEYWORDS: Golgi apparatus, transport carrier, protein kinase D, export kinetics, membrane trafficking.

INTRODUCTION

Secretory proteins synthesized into the lumen of the ER are transported to the Golgi apparatus, where they are further processed and eventually sorted at the *trans*-Golgi network (TGN) for delivery to their respective destinations (Stalder and Gershlick, 2020; Wakana and Campelo, 2021; Spang, 2015; von Blume and Hausser, 2019; Di Martino et al., 2019). The accurate and timely export of cargo proteins – such as collagens, hormones or neurotransmitters – is essential for the maintenance of cell and tissue homeostasis. Accordingly, errors in this process can have severe physiological and pathophysiological consequences (Zappa et al., 2018). Despite the importance of this process, the molecular machinery and the mechanisms of cargo sorting at the TGN remain largely elusive (Guo et al., 2014; Boncompain and Weigel, 2018; Ford et al., 2021; Ramazanov et al., 2021). In mammalian cells, lysosomal hydrolases bearing a mannose 6-phosphate are sorted by the mannose 6-phosphate receptors into clathrin-coated vesicles for their transport to the endo-lysosomal system (Kienzle and von Blume, 2014; Braulke and Bonifacino, 2009). By contrast, no protein coats have been identified for most export routes from the TGN – especially for those destined to the cell surface (Stalder and Gershlick, 2020; Wakana and Campelo, 2021) –, which has hampered the identification of cargo receptors or of other sorting modules. The discovery by Malhotra and colleagues of a Ca^{2+}-dependent mechanism for the sorting of a subset of soluble secretory cargoes is beginning to reveal the intricacies of this supposedly receptor-independent process (von Blume et al., 2009; Curwin et al., 2012). This mechanism relies on the coordinated action of various cellular components, including the actin filament-severing protein cofilin (von Blume et al., 2009; Curwin et al., 2012), the Ca^{2+} pump SPCA1 (von Blume et al., 2011; Kienzle et al., 2014), the oligomeric lumenal Ca^{2+}-binding protein Cab45 (Crevenna et al., 2016; von Blume et al., 2012), and the sphingolipid sphingomyelin (SM) (Deng et al., 2016, 2018). The export from the Golgi by this pathway is independent of any coat proteins identified thus far. However, how other soluble cargo proteins are sorted for their export from the TGN remains unknown.

The single-pass type I transmembrane (TM) protein TGN46 – or TGN38 in rodents (Ponnambalam et al., 1996) – has been proposed to function as a secretory cargo receptor (Stanley and Howell, 1993; Jones et al., 1993; Wang et al., 1995; Banting and Ponnambalam, 1997; McNamara et al., 2004; Wang and Howell, 2000; Ramazanov et al., 2021). However, direct evidence for a role of TGN46 in Golgi export is lacking. TGN38 was first identified in rat cells and shown to have a well-defined steady-state localization at the TGN (Luzio et al., 1990). As a result, TGN38 and its orthologues have become extensively employed as TGN marker proteins. The amino acid sequence of rat TGN38 is largely conserved amongst other species, including humans (>80% amino acid identity between rat TGN38 and human TGN46), with highly-conserved cytosolic and TM domains and a somewhat less conserved lumenal

79 domain (>60% overall identity but only ~25% in the bulk of the lumenal domain)
80 (Ponnambalam et al., 1996). Despite having a steady-state TGN localization, TGN38/TGN46
81 rapidly cycles between the TGN and the plasma membrane (PM), exiting the TGN in specific
82 carriers called CARTS (carriers of the TGN to the cell surface) (Wakana et al., 2012) and
83 recycling from the PM back to the Golgi via early endosomes (Banting and Ponnambalam,
84 1997; Bos et al., 1993; Rajasekaran et al., 1994; Mallet and Maxfield, 1999; Humphrey et al.,
85 1993). CARTS were first identified by immuno-isolation of TGN46-containing transport
86 carriers from the TGN to the PM (Wakana et al., 2012). CARTS are formed in a protein kinase
87 D (PKD)-dependent manner and contain the Rab6/Rab8 GTPases. CARTS traffic specific
88 secretory cargoes, such as pancreatic adenocarcinoma upregulated factor (PAUF) and lysozyme
89 C (LyzC), while exclude others, such as collagen I or vesicular stomatitis virus G-protein
90 (VSVG) (Wakana et al., 2012, 2013; Wakana and Campelo, 2021; Lujan et al., 2021). However,
91 how secretory cargoes are sorted and specifically packed into CARTS is yet to be understood.
92 Furthermore, whether TGN46 plays an active role in CARTS biogenesis or it is just a passive
93 transmembrane cargo of this pathway is still unknown.

94 Here, we demonstrate that TGN46 plays a key role in constitutive protein secretion, specifically
95 in the sorting of the soluble cargo protein PAUF into CARTS for TGN export. Our data reveal
96 that the topological determinants that describe the proper intracellular and intra-Golgi
97 localization of TGN46, as well as its own incorporation in CARTS, are mainly contained in its
98 lumenal domain. Notably, we find that the lumenal domain of TGN46 is both necessary and
99 sufficient for the export of cargo proteins into CARTS and, moreover, that this domain mediates
100 the cargo sorting function of TGN46. Altogether, our data suggest an essential role for TGN46
101 in the sorting of cargo proteins into transport carriers (CARTS) at the TGN.

102

103 **RESULTS**

104 **TGN46 is required for cargo sorting into CARTS**

105 As TGN46 has been suggested, but not shown, to function in cargo sorting at the TGN, we
106 decided to test this hypothesis. We generated a TGN46-lacking line of HeLa cells by
107 CRISPR/Cas9-mediated knock out of *TGOLN2* – the gene encoding for human TGN46
108 (TGN46-KO cell line) (***Fig. 1A*** and ***Fig. S1A***). To test if TGN46 is required for CARTS-
109 mediated secretion, we transiently expressed a CARTS-specific soluble cargo protein, PAUF-
110 MycHis, in both parental and TGN46-KO cells. Both the medium and cell lysates were
111 collected and analyzed by western blotting with an anti-Myc antibody to detect the secreted and
112 internal PAUF-MycHis pools, respectively. In TGN46-KO cells, PAUF-MycHis secretion was
113 reduced by ~75% as compared to control cells (***Fig. 1A***). We noticed the appearance of a lower

114 molecular weight form of PAUF-MycHis in the lysate of TGN46-KO cells (***Fig. 1A***),
115 suggesting that the processing (e.g., glycosylation) of intracellularly accumulated PAUF-
116 MycHis is incomplete, and opening the possibility of a role for TGN46 in facilitating cargo
117 glycosylation. Immunofluorescence microscopy of cells expressing PAUF-mRFP revealed its
118 presence in a perinuclear compartment in both parental and TGN46-KO cell lines, indicating
119 that PAUF-mRFP efficiently exits the ER in the absence of TGN46 (***Fig. S1A***).

120 To test whether TGN46 is specifically involved in the secretion of CARTS-mediated cargoes
121 or rather plays a general role in TGN export, we simultaneously monitored Golgi export of
122 PAUF-mRFP (a CARTS cargo) and VSVG-HA (a non-CARTS cargo) (Wakana et al., 2012;
123 Wakana and Campelo, 2021) in parental and TGN46-KO cells. We used the standard
124 temperature-induced block in cargo export at the TGN to monitor synchronous exit of VSV-G
125 or PAUF in control and TGN46-lacking cells. Cells were first incubated at 20ºC for 2h to block
126 TGN export, and subsequently shifted to 37ºC for 15 min to allow for synchronized export from
127 the TGN, after which cells were fixed and the number of cargo-containing vesicular structures
128 per unit area was analyzed by confocal fluorescence microscopy (***Fig. 1B*** and ***Fig. S1B***). Our
129 data show that the number density of PAUF-mRFP-positive punctate structures – which define
130 CARTS (Wakana et al., 2012) – is significantly reduced by ~50% in TGN46-KO cells as
131 compared to parental cells (***Fig. 1B***). These results agree with and complement the observed
132 inhibition of PAUF secretion in the absence of TGN46 (***Fig. 1A***). By contrast, the number
133 density of VSVG-containing carriers was unaltered upon TGN46 depletion (***Fig. 1B*** and ***Fig.***
134 ***S1B***), indicating that TGN46 selectively functions in the export of a subset of cargo proteins at
135 the TGN. In addition, TGN46 depletion did not increase the proportion of CARTS (defined as
136 carriers positive for PAUF) that also contained VSVG (***Fig. S1C***). These data strongly suggest
137 that, in the absence of TGN46, PAUF is not re-routed towards alternative TGN export routes
138 (particularly to that of VSV-G-containing transport carriers), and therefore bona fide CARTS
139 are still formed, although at a strongly reduced rate. Hence, we will use PAUF as a marker
140 protein for CARTS throughout this article.

141 We next assessed by fluorescence loss in photobleaching (FLIP) microscopy the residence time
142 of PAUF in the Golgi apparatus, which is a dynamic measure of the Golgi export rate of this
143 cargo (***Fig. S1D***). In our FLIP experiments, we systematically photobleached by using a high
144 intensity laser the entire pool of fluorescent protein (e.g., PAUF-mRFP) located outside of the
145 perinuclear Golgi area, and measured the decay of the fluorescence intensity of the Golgi area
146 as function of time (***Fig. S1D***). Thus, for cargo proteins that are rapidly exported from the
147 Golgi, the fluorescence intensity in the Golgi area is expected to rapidly decay, whereas for
148 resident Golgi proteins, the fluorescence should decay more slowly. A variant of FLIP
149 microscopy, known as inverse fluorescence recovery after photobleaching (iFRAP)

150 microscopy, has been previously used to monitor the dynamics of Golgi export (Hirschberg et
151 al., 1998; Patterson et al., 2008). The main distinction between iFRAP and FLIP lies in the
152 frequency of photobleaching. While in iFRAP, photobleaching is performed only once at the
153 beginning of the experiment, FLIP involves repeated photobleaching (FLIP is sometimes also
154 referred to as "repeated iFRAP") (Ishikawa-Ankerhold et al., 2012). Our FLIP results showed
155 that PAUF-mRFP has a longer Golgi residence time in TGN46-KO cells (~40 min) as compared
156 to control cells (~25 min), and therefore TGN46 is necessary for an efficient and fast export of
157 PAUF (***Fig. 1C,D*** and ***Fig. S1D***). Taken together, our results indicate that TGN46 is necessary
158 for CARTS-mediated PAUF export from the TGN.

159 **TGN46 is required for cargo loading into CARTS**

160 Cargo-loaded CARTS detach from the TGN once the neck of the nascent carrier is severed
161 through a membrane fission reaction, a process regulated by the kinase activity of PKD
162 (Wakana et al., 2012). Accordingly, expression of a kinase-dead mutant of PKD (PKD-KD)
163 leads to the formation of cargo-loaded tubules (fission-defective CARTS precursors) at the
164 TGN (Malhotra and Campelo, 2011; Wakana and Campelo, 2021). We took advantage of this
165 to test if TGN46 is needed for cargo loading into CARTS and/or for membrane bending. We
166 co-transfected PAUF-mRFP and PKD2-KD-Flag in control and TGN46-depleted HeLa cells,
167 after which cells were fixed and processed for immunofluorescence microscopy. We first
168 observed that TGN46 depletion did not affect the number or appearance of PKD2-KD-Flag-
169 positive TGN tubules per cell (***Fig. 1E*** and ***Fig. S1E***), suggesting that TGN46 is not necessary
170 for membrane bending. Next, we observed that in control (TGN46-positive) cells, a large
171 fraction of Golgi tubules contained both TGN46 and PAUF-mRFP (~75±15% of tubules
172 containing PAUF) (***Fig. 1E***), as previously described (Liljedahl et al., 2001; Wakana et al.,
173 2012). In contrast, and remarkably, PAUF-mRFP was absent from the majority of the tubules
174 induced by PKD2-KD-Flag in TGN46-depleted cells (~45±10% of tubules containing PAUF)
175 (***Fig. 1E*** and ***Fig. S1E***). These findings strongly indicate that TGN46 is required for sorting
176 and loading the secretory cargo protein PAUF into nascent CARTS at the TGN.

177 **TGN46 export in CARTS is not dependent on TGN46 cytosolic tail signals**

178 Although a number of sequence motifs have been reported to serve as retention signals for
179 Golgi-resident proteins (Welch and Munro, 2019; Lujan and Campelo, 2021), less is known
180 about how cargoes are selectively sorted into transport carriers budding from the TGN.
181 Particularly, sorting mechanisms for CARTS-specific cargoes remain elusive (Wakana and
182 Campelo, 2021). To investigate how TGN46 sorts cargoes into CARTS, we employed a
183 mutagenesis approach to examine whether TGN46 possesses specific topological determinants
184 (such as domains, regions, or motifs) responsible for its cargo sorting and packaging function.

185 As TGN46 is a single-pass type I TM protein of 437 amino acids (human TGN46, UniProt
186 identifier O43493-2), we investigated whether functional cargo-packaging modules can be
187 found in *(i)* the N-terminal lumenal domain (amino acids 22–381), *(ii)* the single TM domain
188 (TMD; amino acids 382–402), and/or *(iii)* the short C-terminal cytosolic tail (amino acids 403–
189 437). In particular, we generated a battery of mutant proteins and evaluated how they behave
190 in terms of *(i)* their fine intra-TGN protein localization, *(ii)* their specific sorting into CARTS,
191 and *(iii)* their Golgi export rate.

192 We start by investigating the existence of sorting signals in the cytosolic tail of TGN46. This
193 tail region contains a tyrosine-based cytosolic motif (YXXΦ; where X represents any amino
194 acid, and Φ is an amino acid with bulky hydrophobic side chains (Ohno et al., 1996); in TGN46:
195 YQRL, amino acids 430-433). This motif acts as an endocytic signal for PM internalization
196 and trafficking back to the TGN, and is therefore crucial for the steady-state localization of
197 TGN46 at TGN (Banting and Ponnambalam, 1997; Stanley and Howell, 1993; Rajasekaran et
198 al., 1994; Bos et al., 1993; Humphrey et al., 1993; Banting et al., 1998). We expressed in HeLa
199 cells a GFP-tagged deletion mutant of TGN46 lacking the cytosolic domain but maintaining
200 the lumenal domain and TMD (GFP-TGN46-Δcyt) (***Fig. 2A***) and analyzed its intracellular
201 localization by fluorescence microscopy. As previously reported (Bos et al., 1993; Humphrey
202 et al., 1993), GFP-TGN46-Δcyt was partially present at the *trans*-Golgi membranes/TGN and
203 partially at the plasma membrane, as qualitatively seen in the micrographs (***Fig. 2***). We and
204 others have previously shown that the *trans*-Golgi/TGN membranes are laterally
205 compartmentalized into export domains (positive for TGN46) and processing domains (positive
206 for the late-Golgi glycosylation enzyme sialyltransferase, ST) (van Galen et al., 2014; Patterson
207 et al., 2008; Tie et al., 2022). We therefore quantitatively measured whether GFP-TGN46-Δcyt
208 partitions into export or processing subdomains. To that end, we co-expressed either GFP-
209 TGN46 WT or GFP-TGN46-Δcyt together with TGN46-mRFP or ST-mCherry, and measured
210 the degree of perinuclear colocalization between the different protein pairs (Pearson's
211 correlation coefficient (Dunn et al., 2011)) (***Fig. 2B,C***). Our data show that GFP-TGN46-Δcyt
212 has a lower degree of intra-Golgi colocalization with respect to TGN46-mRFP and a higher
213 one with respect to ST-mCherry, as compared to its WT counterpart (***Fig. 2B,C***). Hence, GFP-
214 TGN46-Δcyt shows an intra-Golgi localization pattern more closely resembling that of ST-
215 GFP-positive processing domains (***Fig. 2B,C***). These data indicate that the cytosolic domain of
216 TGN46 confers an overall TGN localization by contributing not only to the recycling from the
217 PM, as previously reported (Bos et al., 1993; Humphrey et al., 1993), but also to its fine steady-
218 state partitioning into TGN export domains and exclusion from processing domains. We next
219 tested how GFP-TGN46-Δcyt is exported from the TGN. We first monitored the incorporation
220 of GFP-TGN46-Δcyt into CARTS. HeLa cells co-overexpressing GFP-TGN46-Δcyt together

221 with either PAUF-mRFP (CARTS marker) or VSVG-HA (a CARTS-independent TM cargo
222 protein) were incubated at 20ºC for 2 h to inhibit TGN export, shifted to 37ºC for 15 min to re-
223 initiate cargo export, fixed, and imaged by fluorescence microscopy. We then analyzed the
224 fraction of cargo-containing carriers (for three different cargoes: GFP-TGN46 WT, VSVG-HA,
225 and GFP-TGN46-Δcyt) that were also positive for PAUF-mRFP (CARTS) or VSVG-HA
226 (VSVG carriers). Our results indicated that GFP-TGN46-Δcyt is preferentially exported in
227 CARTS and not in VSVG carriers, although this mutant cargo protein showed a modest but
228 statistically significant reduction in its CARTS specificity as compared to GFP-TGN46 WT
229 (***Fig. 2D,E***). We next performed FLIP experiments to measure the Golgi residence time of
230 GFP-TGN46-Δcyt, and compare it with that of GFP-TGN46 WT. It is important to emphasize
231 that, owing to the execution of FLIP experiments involving repeated photobleaching of the pool
232 of fluorescent proteins outside the Golgi area, we were able to monitor the actual protein export
233 rate (***Fig. S1D***). This experimental design minimizes the impact of TGN46 recycling back to
234 the TGN, as would occur in iFRAP experiments involving a single photobleaching step.
235 Interestingly, GFP-TGN46-Δcyt exits the Golgi at a rate that is indistinguishable from that of
236 GFP-TGN46 WT (***Fig. 3A,B*** and ***Fig. S2A***). Taken together, our results suggest that, although
237 the cytosolic tail of TGN46 is important for PM recycling, it does not play a major role in
238 mediating TGN46 incorporation into CARTS for export out of the TGN.

239 **TGN46 intra-Golgi localization and CARTS specificity are insensitive to the length and**
240 **composition of its TMD**

241 We next investigated if the information encoded in the amino acid sequence of the TGN46
242 TMD determines its incorporation into CARTS. The hydrophobic matching hypothesis is a
243 TMD-based sorting mechanism that has been proposed to contribute to the retention of Golgi-
244 resident TM proteins (Welch and Munro, 2019; Lujan and Campelo, 2021). This mechanism is
245 based on the hypothesis that single-pass TM proteins preferably partition into membrane
246 regions of a thickness that best matches the hydrophobic length of the protein TMD (Munro,
247 1991; Sharpe et al., 2010; Munro, 1995). The membrane thickness increases along the secretory
248 pathway (Mitra et al., 2004), which correlates with the average TMD length of the proteins of
249 these organelles (Sharpe et al., 2010). Hence, according to the TMD-based retention hypothesis,
250 the separation between Golgi-resident proteins and cargoes destined for export from the TGN
251 is attributed to the distinct physical properties of these domains (Sharpe et al., 2010; Munro,
252 1995; Quiroga et al., 2013; Cosson et al., 2013). TGN46 is a type I protein with a single TMD
253 of 21 amino acids, whereas ST (ST6Gal-I) is a type II protein with a shorter TMD of 17 amino
254 acids (***Fig. 4A***). Thus, we generated two different TGN46 mutants by altering its TMD
255 sequence to test whether the length and/or amino acid composition of the TMD of TGN46 is
256 important for its characteristic intra-Golgi localization, selective CARTS-mediated export, and

257 Golgi residence time. The first mutant (TGN46-shortTMD) is a TGN46 deletion that lacks 4
258 amino acids (AAIL) in the central region of the TMD. For the second mutant (TGN46-ST
259 TMD), we replaced the TGN46 TMD by that of ST, while keeping the topology and, therefore,
260 the correct TMD orientation with respect to the bilayer (***Fig. 4A***). As compared to TGN46 WT,
261 both mutants have shorter TMDs (17 amino acids) and while TGN46-shortTMD maintains the
262 overall amino acid composition, TGN46-ST TMD has a completely altered TMD composition
263 (***Fig. 4A***).

264 First, we expressed different combinations of these proteins in HeLa cells, and monitored their
265 intracellular localization by fluorescence microscopy. Altering the TMD of TGN46 had no
266 discernible impact on intra-Golgi localization (***Fig. 4B,C***), suggesting that the hydrophobic
267 matching mechanism is not a major determinant for the fine intra-Golgi localization of TGN46.
268 Interestingly, even in cells treated with short-chain ceramide (D-ceramide-C6), a treatment that
269 causes morphological changes and the physical segregation of the Golgi membranes into
270 distinct ST- and TGN46-positive Golgi subdomains (Duran et al., 2012; van Galen et al., 2014;
271 Campelo et al., 2017; Capasso et al., 2017), we did not observe any apparent change in the
272 localization of the TGN46 mutants with short TMD with respect to TGN46 WT (***Fig. S3***).
273 However, because our results were obtained using diffraction-limited confocal microscopy
274 (with a spatial lateral resolution of ~250 nm), it is still possible that more subtle alterations in
275 the intra-Golgi localization of these mutants exist at shorter length scales. To address this
276 possibility, we used super-resolution single molecule localization microscopy (SMLM) with a
277 localization precision (resolution) of ~15–30 nm. Our results show that, even with this
278 enhanced spatial resolution, the intra-Golgi localization of the different TGN46 mutants with
279 shorter TMD was indistinguishable from that of TGN46 WT (***Fig. S4***).

280 Second, we asked whether the TGN46 TMD sequence plays a role in dragging this protein into
281 CARTS. Interestingly, the two mutants with shorter TMDs (TGN46-shortTMD and TGN46-
282 ST TMD) lost their preference for being co-packaged with PAUF into CARTS, and partially
283 redirected into other transport carriers such as VSVG carriers (***Fig. 4D,E***), even though they
284 keep a similar steady-state intra-Golgi localization as the TGN46 WT (***Fig. 4A***).

285 Finally, we investigated how fast these TGN46 mutants with shorter TMDs are exported out of
286 the Golgi apparatus. FLIP experiments indicated that the chimeric protein TGN46-ST TMD-
287 GFP has a slower Golgi export rate (longer Golgi residence time) as compared to TGN46-GFP.
288 In addition, TGN46-shortTMD-GFP was exported at a slightly slower rate, although this
289 difference was not statistically significant (***Fig. 3C,D*** and ***Fig. S2B***). Next, we co-
290 overexpressed TGN46-GFP together with TGN46-ST TMD-mRFP or TGN46-mRFP, as a
291 control, and performed FLIP experiments to measure the rate of TGN46 WT-GFP export. The

292 aim of these experiments was to test if the expression of these mutants leads to defects in
293 CARTS biogenesis. Our results show that the Golgi residence time of TGN46-GFP was not
294 affected by the co-expression of either the WT or the chimeric proteins (***Fig. S5A,B***). These
295 data provide further support to the idea that the slower Golgi export rate of TGN46 mutants
296 with short TMDs is a consequence of their compromised selective sorting into CARTS without
297 detectable changes in their intra-Golgi localization.

298 It has been reported that some medial Golgi enzymes can dimerize or oligomerize and that this
299 property (kin recognition) is important for TM protein localization along the Golgi stack
300 (Welch and Munro, 2019; Banfield, 2011; Lujan and Campelo, 2021). However, there are
301 reports showing that kin recognition is not relevant for ST or for other *trans*-Golgi membrane
302 proteins (Munro, 1995). To examine if the unaltered intra-Golgi localization of TGN46-
303 shortTMD and TGN46-ST TMD compared to WT was due to protein
304 dimerization/oligomerization, we tested whether TGN46-GFP and TGN46-mRFP co-
305 immunoprecipitated when expressed in HeLa cells. Our results show no obvious dimerization
306 between TGN46-GFP and TGN46-mRFP (***Fig. S5C***).

307 One of the possible consequences of shortening the TMD of TGN46 might be the partial burial
308 of the highly charged residues of TGN46 cytosolic tail into the cytosolic leaflet of the TGN
309 membrane, which, concomitantly, could negatively hamper its CARTS-mediated export. If so,
310 the observed phenotype would follow from the unnatural proximity of the cytosolic tail to the
311 membrane rather than from a direct effect due to hydrophobic mismatch. To test this hypothesis,
312 we deleted the cytosolic tail of TGN46-ST TMD – which, as we showed earlier (***Fig. 2***), has
313 no major effect in TGN46 export in CARTS – to generate a mutant with TGN46 lumenal
314 domain, ST TMD, and no cytosolic tail (TGN46-Δcyt-ST TMD, ***Fig. 2A***). This chimeric
315 protein phenocopies GFP-TGN46-Δcyt regarding its *(i)* intra-Golgi localization (***Fig. 2B,C*** and
316 ***Fig. 4B,C***), and *(ii)* CARTS specificity (***Fig. 2D,E*** and ***Fig. 4D,E***), with only a milder reduction
317 in the Golgi export rate (***Fig. 3A,B*** and ***Fig. S2A***). Taken together, these results strongly
318 indicate that the hydrophobic matching mechanism (as well as the information encoded in the
319 TMD) does not play a primary role in driving the intra-Golgi localization and Golgi export of
320 TGN46.

321 **The lumenal domain of TGN46 is necessary and sufficient for CARTS-mediated export**
322 **from the TGN**

323 Finally, we enquired if the lumenal domain of TGN46 plays a role in intra-Golgi localization,
324 Golgi export rate (residence time), and selective sorting into CARTS. First, we aimed to test
325 whether the lumenal domain of TGN46 is *necessary* for its sorting and packaging into CARTS.
326 We thus generated a deletion mutant of TGN46 lacking its lumenal domain (GFP-TGN46-

327 Δlum) (***Fig. 5A***), expressed it in parental HeLa cells, and monitored its intra-Golgi localization
328 by fluorescence microscopy. Although still perinuclear, GFP-TGN46-Δlum lost the
329 characteristic intra-Golgi localization of the TGN46 WT and rather localized into ST-mCherry-
330 positive processing domains of the *trans*-Golgi membranes (***Fig. 5B,C***). Notably, this exclusion
331 from TGN export domains paralleled a striking reduction in the selective incorporation of GFP-
332 TGN46-Δlum into CARTS (***Fig. 6A,B***), as well as in the rate of Golgi export (***Fig. 3F*** and ***Fig.***
333 ***S6A,C***), as compared to the full length protein. These results consistently indicate that the
334 lumenal domain of TGN46 is *necessary* for CARTS-mediated export of TGN46, therefore
335 suggesting that this domain contains a signal for sorting and loading into CARTS.

336 Next, we asked whether the TGN46 lumenal domain is not only necessary but also *sufficient*
337 for CARTS-mediated TGN exit. We started by generating a soluble cargo protein that only
338 contains the lumenal domain of TGN46, tagged with GFP at the N terminus just following the
339 signal sequence (GFP-TGN46lum) (***Fig. 5A***). Upon expression in HeLa cells, GFP-TGN46lum
340 localizes to the Golgi apparatus where it only shows a partial colocalization with TGN46-mRFP
341 or with ST-mCherry (***Fig. 5B,C***). This low degree of colocalization could be due to the fact
342 that we are comparing the location of soluble and TM proteins. Nonetheless, when we used our
343 synchronized cargo release assay to measure selective incorporation into CARTS, GFP-
344 TGN46lum maintained specificity for CARTS-mediated export (***Fig. 6A,B***). Moreover, FLIP
345 experiments revealed that GFP-TGN46lum exits as fast as GFP-TGN46 WT, or even faster
346 (***Fig. 3E*** and ***Fig. S6A,B***). We next asked if the signal encoded in the TGN46 lumenal domain
347 can direct otherwise unrelated proteins into CARTS. In particular, we tested whether TGN46
348 lumenal domain can lead to CARTS-mediated export of *(i)* a Golgi-resident TM protein (ST),
349 and *(ii)* a CARTS-independent TM cargo protein (VSVG). To that end, we exchanged the
350 lumenal domains (while maintaining the correct topology) of ST and VSVG for that of TGN46,
351 thereby generating two chimeric constructs: GFP-ST-TGN46lum, and GFP-VSVG-
352 TGN46lum, respectively (***Fig. 5A***). We then studied the intra-Golgi localization, CARTS-
353 mediated export selectivity, and Golgi export rate of these proteins in relation to their WT
354 counterparts. Our results indicate that GFP-ST-TGN46lum maintained a good degree of
355 colocalization with ST-mCherry and additionally it increased its colocalization with TGN46-
356 mRFP (***Fig. 5B,C***). Similar results were obtained for the intra-Golgi localization of GFP-
357 VSVG-TGN46lum with respect to TGN46-mRFP and VSVG-HA (***Fig. 5D,E***). As an
358 additional control to eliminate any sources of possible intra-Golgi sorting signals residing in
359 the lumenal region of VSVG, we also included GFP-VSVG-Δlum – a deletion mutant of VSVG
360 lacking the lumenal domain (***Figure 5A***). This construct shows a reduced colocalization with
361 respect to both TGN46-mRFP and VSVG-HA, possibly indicating a tug-of-war between
362 lumenal signals – driving localization towards TGN46-positive export domains – and

363 TM/cytosolic signals – driving localization towards VSVG-positive export domains (***Fig.***
364 ***5D,E***). Despite these subtle differences in their intra-Golgi localization, the GFP-VSVG-
365 TGN46lum chimera specifically exits the TGN in CARTS, with a similar specificity to that of
366 TGN46-GFP, whereas GFP-VSVG-Δlum exits in VSVG carriers, similarly to VSVG-GFP
367 (***Fig. 6A,B***). In line with these observations, FLIP microscopy showed a fast Golgi export rate
368 of GFP-VSVG-TGN46lum, indistinguishable from that of GFP-TGN46 WT, and a somewhat
369 slower export rate for both GFP-VSVG-Δlum and VSVG-GFP (***Fig. 3F,G*** and ***Fig. S6A,C,D***).
370 These results indicate that the lumenal domain of TGN46 can re-direct other TM cargo proteins
371 into CARTS, thereby acting as a gain-of-function domain for fast export in CARTS out of the
372 Golgi apparatus. Similarly, fusing the lumenal domain of TGN46 to ST also created an export-
373 competent protein that exits the TGN by being specifically sorted into CARTS (***Fig. 6A,B***).
374 Remarkably, GFP-ST-TGN46lum has a shorter Golgi residence time as compared to ST-GFP,
375 with an export rate slightly slower but comparable to that of GFP-TGN46 WT (***Fig. 3F*** and
376 ***Fig. S6A,C***). Altogether, these results indicate that, as long as the protein is correctly localized
377 within the Golgi membranes, signals encoded in the lumenal domain of TGN46 are not only
378 necessary, but also *sufficient* for cargo sorting into CARTS.

379 **Correlation between CARTS specificity and Golgi export rate of cargo proteins**

380 Our data thus far suggest that proteins with a high specificity for the CARTS export pathway
381 have a relatively fast Golgi export rate (***Figs. 2–6***). To quantitatively illustrate these findings,
382 we plotted for each of the tested cargo proteins their CARTS specificity as a function of their
383 Golgi residence time. The plots reveal the existence of a negative correlation between CARTS
384 specificity and Golgi residence time (slope~-0.9±0.4% min^{-1}, r^2~0.4) (***Fig. 7A***). Both TGN46
385 WT (***Fig. 7A***, dark green) and the different chimeric cargo proteins that contain the lumenal
386 domain but not the cytosolic tail of TGN46 (***Fig. 7A***, light green and light blue) are selectively
387 sorted into CARTS (>50% specificity) and rapidly exported out of the Golgi (short Golgi
388 residence times ~10–30 min). Interestingly, in the absence of the lumenal domain of TGN46
389 (***Fig. 7A***, red) or when only the TMD sequence of TGN46 is altered (while keeping the WT
390 cytosolic tail) (***Fig. 7A***, yellow), cargoes lost CARTS specificity (<35%) with the concomitant
391 decrease in the Golgi export rate (larger Golgi residence times ~30–50 min), consistent with
392 the values found for VSVG (***Fig. 7A***, blue), a cargo that is excluded from CARTS (Wakana et
393 al., 2012) and shows a slower Golgi export rate (Golgi residence time ~30 min). Taken together,
394 these data indicate that VSVG-containing carriers mediate a relatively slower Golgi export
395 route as compared to CARTS, thereby underscoring the different export kinetics of distinct
396 Golgi export routes.

397 **The cargo sorting function of TGN46 is mediated by its lumenal domain**

398 TGN46 is a bona fide CARTS component (Wakana and Campelo, 2021), and our data indicate
399 that it is required for PAUF sorting into CARTS for secretion (***Fig. 1***). Furthermore, we have
400 shown that the lumenal domain of TGN46 is necessary and sufficient for the incorporation of
401 this TM protein into CARTS (***Fig. 5,6***). Thus, it is plausible that TGN46 facilitates the sorting
402 of client cargoes via its lumenal domain. To test this hypothesis, we investigated whether the
403 expression of different mutants of TGN46 rescues the sorting and export defect we have
404 observed in TGN46-KO cells. In particular, we studied the following TGN46-based proteins:
405 GFP-TGN46 (wild type protein), GFP-TGN46-Δcyt (no cytosolic tail), GFP-TGN46-ST TMD
406 (TGN46 with the shorter TMD of the Golgi resident ST), and GFP-TGN46-Δlum (no lumenal
407 domain). First, TGN46-KO cells co-expressing any of these TGN46 constructs together with
408 PAUF-mRFP or VSVG-HA were synchronized by a 20ºC block and 15 min release at 37ºC,
409 after which the cells were fixed and prepared for fluorescence microscopy (***Fig. S7A***). We
410 quantified the percentage of carriers containing the different TGN46 mutants that were also
411 positive for either PAUF-mRFP (CARTS marker) or VSVG-HA (non-CARTS marker) and
412 compared those to the distributions found when the same proteins were expressed in the
413 parental HeLa cells (***Fig. 7B***; see also ***Fig. 2E, 4E, 6B***). Our results indicate that CARTS
414 selectivity of these cargo proteins was not severely altered in the TGN46 KO cells as compared
415 to the parental cell line. Next, we carried rescue experiments by performing FLIP in TGN46-
416 KO cells expressing PAUF-mRFP together with GFP-TGN46, GFP-TGN46-Δcyt, TGN46-ST
417 TMD-GFP, or GFP-TGN46-Δlum to measure the rate of PAUF-mRFP export from the Golgi.
418 Interestingly, overexpression of GFP-TGN46 WT or GFP-TGN46-Δcyt – but not of TGN46-
419 ST TMD-GFP or GFP-TGN46-Δlum – was able to rescue PAUF-mRFP export from the Golgi
420 in TGN46-KO cells (***Fig. 7C,D*** and ***Fig. S8***). Taken our data together, we propose a model in
421 which the proper partitioning of TGN46 into TGN export domains (sites of CARTS biogenesis)
422 is required for its lumenal domain to efficiently recruit and sort PAUF and possibly other
423 CARTS cargoes into nascent transport carriers for secretion.

424

425 **DISCUSSION**

426 **TGN46 is necessary for cargo loading into CARTS**

427 Here, we revealed a novel role for TGN46 in the sorting of the secretory cargo protein PAUF
428 into nascent transport carriers at the TGN. CRISPR/Cas9-edited HeLa cells lacking TGN46
429 showed *(i)* a drastic inhibition in PAUF secretion (***Fig. 1A***); *(ii)* a reduction in the number of
430 cytoplasmic CARTS – but not of other TGN-to-PM carriers such as VSVG carriers – (***Fig. 1B***);
431 and *(iii)* a decrease in the Golgi export rate of PAUF (***Fig. 1C,D***). To investigate the role of
432 TGN46 in TGN export, we took advantage of the phenotype created by the exogeneous

433 expression of PKD-KD, which consists in the presence of long, cargo-containing tubules
434 emanating from the TGN membranes (Liljedahl et al., 2001). Because these tubules are fission-
435 defective transport carriers, and membrane fission is downstream of cargo sorting, we could
436 use this assay as a useful approach to investigate cargo sorting into PKD-dependent transport
437 carriers at the TGN. Our results showed that TGN46 is not necessary for membrane tubulation
438 but it is essential to sort and package the secretory cargo PAUF into PKD-KD-induced TGN
439 tubules (***Fig. 1E***), therefore suggesting a prime role of TGN46 in cargo sorting. Indeed, TGN46
440 (and its rodent orthologs TGN38/TGN41) had previously been suggested to act as a cargo
441 receptor, based on the fact that this protein shares the characteristics of a typical cargo receptor:
442 it is a type-I single-pass TM protein that cycles between the TGN and the PM (Stanley and
443 Howell, 1993). Although future work will be necessary to pinpoint the mechanism that TGN46
444 uses for cargo sorting and loading into carriers, we believe that the data reported here shed
445 some light into the actual role of human TGN46 for the sorting and loading of cargo proteins
446 into TGN-derived transport carriers destined to the cell surface.

447 It is important to underscore that our findings using the TGN46 KO cell line reveal a partial
448 inhibition rather than a complete block in PAUF export (***Fig. 1A,C,D*** and ***Fig. 7C,D***). This
449 incomplete block may stem from various factors. *First*, cells may respond to genetic
450 perturbations, such as those induced by a gene knockout, by adapting to compensate the loss of
451 a specific gene. These compensatory mechanisms could potentially mitigate the full impact of
452 TGN46 depletion, providing a plausible explanation for the observed partial effects. *Second*,
453 our data indicate that the absence of TGN46 reduces PAUF secretion without completely
454 inhibiting its export (***Fig. 1A***). These results align with our proposed role for TGN46 in cargo
455 sorting. In the absence of TGN46, secretory cargo proteins might find alternative, TGN46-
456 independent routes for export, such as through bulk flow or uncontrolled incorporation into
457 other transport carriers. Indeed, the partial redistribution of the TGN46-Δlum mutant into
458 VSVG carriers (***Fig. 6B***) supports this possibility. Notably, similar situations have been
459 observed when unrelated sorting factors were depleted from the Golgi membranes. For
460 instance, disruption of the cofilin/SPCA1/Cab45 sorting pathway inhibits the secretion of
461 pathway clients but does not bring this effect to a complete halt (von Blume et al., 2011, 2012).
462 And *third*, it is possible that TGN46 is not the sole player in the sorting of PAUF into CARTS.
463 The presence of redundant or alternative mechanisms cannot be ruled out.

464 Although in here we have focused on the study of the model CARTS cargo protein PAUF, it
465 seems reasonable to expect that TGN46 is responsible for the sorting of other CARTS cargoes.
466 Interestingly, the lumenal domain of TGN38 has been shown to interact with the adhesion
467 receptor integrin $ß_1$ and to partially co-localize with integrins $α_5$ and $ß_1$, but not $α_V$ or $ß_3$ (Wang
468 and Howell, 2000). In addition, TGN38 regulates cell adhesion, as the overexpression of

469 TGN38 leads to cell detachment from the substrate (Luzio et al., 1990; McNamara et al., 2004;
470 Lee and Banting, 2002; Humphrey et al., 1993; Reaves et al., 1993). Remarkably, integrin $ß_1$ is
471 transported from the TGN to the cell surface in a Rab6-mediated (Huet-Calderwood et al.,
472 2017) and PKD-dependent manner (Yeaman et al., 2004). Because CARTS are PKD-dependent
473 transport carriers that share many similarities with Rab6-positive carriers (Wakana and
474 Campelo, 2021), we propose that the role of TGN46 as a cargo receptor for the sorting of the
475 soluble CARTS-specific cargo PAUF is quite general, and can include a long list of both soluble
476 and TM cargo proteins, such as $\alpha_5ß_1$ integrins. Interestingly, TGN46 binds a cytosolic protein
477 complex made of 62 kDa protein (p62) and Rab6 (Jones et al., 1993). These authors used a
478 Golgi budding assay to test the involvement of the cytosolic domains of TGN38 and TGN41 in
479 budding of Golgi-derived carriers that contain the transmembrane cargo protein pIgA-R
480 (polymeric IgA-receptor). The authors showed that the budding of these carriers was blocked
481 upon incubation of the Golgi membranes with peptides against the cytosolic tail of TGN38/41.
482 These data complements and contrasts our data showing that the cytosolic tail of TGN46 is
483 dispensable for PAUF sorting into CARTS. It thus appears possible that TGN46 plays a
484 multifaceted role in TGN export by controlling the export of soluble and transmembrane cargo
485 proteins through alternative mechanisms.

486 In addition, TGN46 has been recently reported to assist in the trafficking of severe acute
487 respiratory syndrome coronavirus 2 (SARS-CoV-2), as this protein is upregulated in SARS-
488 CoV-2-infected cells and cells depleted of TGN46 showed a reduced SARS-CoV-2 infection
489 rate (Zhang et al., 2022). In summary, further work will be required to grasp the full magnitude
490 of the role of TGN46 in protein sorting for export and secretion out of the TGN, which can
491 provide ideas to help in the rational design of new therapeutic tools to target human pathologies
492 associated with secretion defects.

493 **TGN46 localization to *trans*-Golgi membranes is independent of TMD length and**
494 **composition**

495 Different mechanisms that mediate the spatial and temporal organization of Golgi residents
496 (e.g., glycosylation enzymes) and their respective substrates (e.g., secretory cargoes) have been
497 proposed (Banfield, 2011; Welch and Munro, 2019; Lujan and Campelo, 2021). Amongst these,
498 a lipid-based retention/sorting mechanism has been proposed for Golgi TM proteins (Patterson
499 et al., 2008; Munro, 1991; Sharpe et al., 2010; Munro, 1995; Lippincott-Schwartz and Phair,
500 2010). This mechanism builds on the observation that the levels of certain lipids, such as
501 cholesterol and SM, are enriched along the *cis*- to *trans*- axis of the Golgi stack (Van Meer et
502 al., 2008; Bretscher and Munro, 1993). This lipid gradient correlates with an increase in the
503 thickness of those membranes (Mitra et al., 2004). In addition, a comprehensive bioinformatic

504 study using large datasets of TM proteins from different organisms showed a correlation
505 between the intracellular localization of these proteins and different specific features of their
506 TMDs, such as their length, which on average is shorter for proteins of the early secretory
507 pathway as compared to those of the late secretory pathway (Sharpe et al., 2010). Furthermore,
508 it has been proposed that not only the TMD length but also the distribution of bulky and highly
509 hydrophobic amino acids within the TMD affect the specific location of TM proteins (Sharpe
510 et al., 2010; Quiroga et al., 2013). Altogether, these studies have led to the suggestion of the
511 hydrophobic matching model, which proposes that gradients in bilayer thickness along the
512 membranes of the secretory pathway contribute/drive the sorting and retention of TM proteins
513 across the secretory pathway. Although there is compelling evidence for a TMD-based
514 mechanism for targeting certain TM proteins to specific cell surface domains (Milovanovic et
515 al., 2015), to localize type-II resident proteins of the cell surface and the Golgi membranes
516 (Munro, 1995; Quiroga et al., 2013), and also to sort the type-III TM protein linker for
517 activation of T-cells (LAT) by raft-mediated partitioning (Diaz-Rohrer et al., 2014; Lorent et
518 al., 2017; Castello-Serrano et al., 2023), it remained unclear how this mechanism contributed
519 to the retention, sorting and lateral segregation of Golgi resident enzymes and their substrates.
520 Interestingly, by using a coarse-grained mathematical model of intra-Golgi transport, Dmitrieff
521 et al. showed that experimental data on the Golgi dynamics of secretory cargoes and Golgi
522 residents cannot be explained if the hydrophobic matching mechanism is the sole retention
523 mechanism for Golgi residents (Dmitrieff et al., 2013). In agreement with this latter proposal,
524 our results revealed that hydrophobic mismatch between TMDs and bilayer thickness is not
525 sufficient to drive the sorting of a TM Golgi-resident enzymes from substrate cargoes along the
526 *trans*-Golgi/TGN membranes. Specifically, we studied the role of TMD length and amino acid
527 composition in intra-Golgi localization of the type-I single-pass TM cargo glycoprotein
528 TGN46, and observed that localization and sialylation of TGN46 is not affected when its TMD
529 is shortened or even replaced by that of the Golgi-resident type-II TM enzyme ST (***Fig. 4A–***
530 ***C***). These data suggest that the hydrophobic length and amino acid composition of the TMD of
531 TGN46 is not a major contributing factor to localize this TM protein into Golgi export domains
532 for its function in sorting and packaging of soluble cargoes into nascent CARTS.

533 **A role for the cytosolic tail of TGN46 in driving its proper intra-Golgi localization**

534 Our results indicate that the cytosolic tail of TGN46 contains a specific signal allowing the
535 perinuclear pool of TGN46 to localize in the right sub-compartment within the TGN
536 membranes. In particular, the localization of a TGN46 mutant lacking the cytosolic tail was
537 shifted towards Golgi processing domains (ST enzyme-positive regions) rather than in export
538 domains (TGN46 WT-positive regions) (***Fig. 2B,C***). It has been well documented that the
539 cytosolic tail of TGN38 – the rodent ortholog of TGN46 – contains a tyrosine-based motif for

540 internalization and recycling of the protein back to the TGN (Bos et al., 1993; Humphrey et al.,
541 1993). Adding to these earlier reports, our data suggest that the cytosolic tail of TGN46 also
542 determines its fine intra-Golgi localization. Factors such as Vps74/GOLPH3 or coat proteins
543 such as COPI (Tu et al., 2008; Wood et al., 2009; Welch et al., 2021), influence enzyme-cargo
544 interaction/segregation by recognizing cytoplasmic signals and thereby inducing protein
545 retention by fast recycling. In addition, SM metabolism can also contribute to laterally organize
546 the Golgi membranes at the nanoscale for efficient cargo-enzyme interactions (Duran et al.,
547 2012; van Galen et al., 2014).

548 **Cargoes destined for secretion exit the Golgi with different export rates**

549 We observed that the Golgi residence time of different TGN46-based chimeric proteins was
550 different depending on the specific export route they use to exit the TGN (***Fig. 7A***). In
551 particular, when we compared the export rate of two different PKD-dependent TM proteins
552 (TGN46, which is exported in CARTS; and VSVG, which is not), we found that CARTS appear
553 to be a faster export route (~15 min Golgi residence time) than VSVG carriers (~30 min Golgi
554 residence time) (***Fig. 7A***). Remarkably, when we generated a series of chimeras combining
555 different domains from different proteins, we observed that loss of CARTS specificity
556 correlated with larger Golgi residence times (***Fig. 7A***). These results could provide an
557 explanation as to why cells use different routes (with different machineries) for the export of
558 secretory or TM cargo proteins to the same destination, *i.e.*, different cargoes might require
559 longer/shorter residence times in the Golgi and/or faster transport kinetics to the cell surface. It
560 is possible that developing various TGN-to-PM export routes of different kinetics might have
561 endowed cells with beneficial mechanisms to cope with their secretory needs under stress
562 conditions.

563 CARTS have been suggested to be enriched in cholesterol and SM (Wakana et al., 2021;
564 Wakana and Campelo, 2021), and their biogenesis to require intact ER-Golgi membrane
565 contact sites (MCS) supplying the TGN with these lipids (or their precursors) (Wakana et al.,
566 2015, 2021). Notably, data from Deng, Pakdel et al. suggested that TGN46 is a native cargo of
567 the SM-dependent TGN export pathway, as it was identified by mass spectrometry to be co-
568 packaged in carriers containing the lumenal SM sensor EQ-SM-APEX2 (Deng et al., 2018).
569 Given the similarities between the SM/Cab45 and CARTS export pathways (Stalder and
570 Gershlick, 2020; Wakana and Campelo, 2021), it is tempting to speculate that TGN46 could be
571 enriched in ER-Golgi MCS and perhaps complement the sorting function of Cab45 for a subset
572 of secretory cargo proteins.

573 Further elaborating on these specific needs/characteristics of different cargoes/export routes
574 will be of outmost importance in the future to better understand the intricate relationships

575 between physiological needs and the regulation of the secretory machinery of the cell (Di
576 Martino et al., 2019; Luini and Parashuraman, 2016; Cancino et al., 2013; Wakana and
577 Campelo, 2021).

578

579 **IDEAS AND SPECULATIONS**

580 In the following, we would like to propose some ideas and speculate on a possible mechanism
581 by which TGN46 could serve as a cargo sorting factor at the TGN. Our data suggest that the
582 lumenal domain of TGN46 might have a propensity to self-associate, because *(i)* the steady-
583 state intra-Golgi localization of TGN46 is lost when the lumenal domain is deleted (***Fig. 5B,C***);
584 and *(ii)* although the soluble lumenal domain of TGN46 showed an intermediate intra-Golgi
585 localization phenotype, anchoring this domain to the membrane by fusing it to the *trans*-Golgi-
586 targeting sequence of ST conferred this chimera a localization pattern indistinguishable from
587 that of full length TGN46 (***Fig. 5B,C***). To obtain insights on how this might occur, we analyzed
588 the sequence features of the lumenal domain of TGN46 (***Fig. S9A***). On the one hand, TGN46
589 is a heavily glycosylated protein, including 9 predicted *N*-linked glycosylation sites, multiple
590 *O*-linked glycosylation sites, as well as 5 phosphosites (***Fig. S9B***), all of them located at the
591 lumenal domain. Structurally, this region is highly disordered, as evidenced by a high PONDR
592 score (in the range 0.5–1) for most of its amino acid sequence (***Fig. S9C***), indicating with high
593 probability that the lumenal domain of TGN46 is an essentially intrinsically disordered region
594 (IDR). In recent years, IDR of various proteins have been shown to have the capacity to form
595 biomolecular condensates (Banani et al., 2017; Garcia-Cabau and Salvatella, 2021; Shin and
596 Brangwynne, 2017; Hyman et al., 2014; Brangwynne et al., 2009; Case et al., 2019; Mittag and
597 Pappu, 2022). Due to their liquid nature, these condensates take spherical shapes, and their
598 components are mobile within the condensate (dense phase) and can also exchange with those
599 present, at a lower concentration, in the external solution (light phase). Carefully testing
600 whether the TGN46 lumenal domain has the capacity to form liquid droplets *in vitro* and in a
601 cellular context will be necessary to hypothesize that condensate formation assisted by TGN46
602 lumenal domain could mediate the sorting of secretory cargoes into transport carriers for their
603 secretion. Naturally, these ideas still remain highly speculative but they help us ask a number
604 of interesting questions. First, what is the role of TGN46 lumenal domain glycosylation in its
605 sorting function, and, potentially, in the hypothetical regulation of droplet/condensate
606 formation? Interestingly, the levels of the cation-dependent mannose 6-phosphate receptor – a
607 well-known cargo receptor at the TGN for the sorting of lysosomal hydrolases into clathrin-
608 coated vesicles – are about 10-fold higher than those of TGN46: ~200,000 copies vs. ~30,000
609 copies, respectively, per HeLa cell (Kulak et al., 2014). Of notice, our co-immunoprecipitation

experiments showed no evidence for strong TGN46-TGN46 protein interactions (***Fig. S5C***), which agrees with the possibility of TGN46 forming biomolecular condensates that are stabilized by weak interactions. It is therefore tempting to speculate that the mechanism of cargo sorting by TGN46 might be different from that of a classical cargo receptor, such as the mannose 6-phosphate receptor, which binds its clients in an ~1:1 stoichiometry. It still remains unknown whether PAUF is recruited to nascent CARTS by the lumenal domain of TGN46. PAUF is a putative lectin, so it is possible that it interacts with TGN by recognizing the glycans on its lumenal domain (***Fig. S9B***). Alternatively, or in parallel, TGN46 condensates could be liquid droplets with a specific chemical microenvironment (pH, Ca^{2+} concentration, etc.), which might serve to recruit certain cargoes. Future endeavors along these lines will help elucidate the mechanistic details of cargo sorting by TGN46.

Remarkably, Parchure et al. recently showed that liquid-liquid phase separation (LLPS) might play a dominant role in the formation of secretory insulin-containing granules for regulated exocytosis (Parchure et al., 2022). The authors showed that the chromogranins – key regulators of secretory granule formation – can undergo LLPS *in vitro* in conditions of low pH, such as the one found in the TGN. Notably, cargoes such as proinsulin or LyzC do co-partition with chromogranins in liquid droplets, and put forward a "client sponge" model in which secretory cargoes would be sorted into liquid biomolecular condensates based on their size.

CONCLUSION

In summary, we presented here experimental results that support a model in which TGN46 serves as a sorting receptor for a subset of cargoes at the TGN. Thanks to TGN46, these cargoes are sorted packaged into nascent CARTS for their fast delivery to the cell surface or for secretion outside the cell. The sorting capabilities of TGN46 are ascribed to its lumenal domain, an IDR prone to undergo phase separation. Based on our findings, we propose a working model in which TGN46 functions to recruit secretory cargoes in the lumen of the TGN for their sorting and fast export to the cell surface by CARTS.

ACKNOWLEDGMENTS

We thank members of the Single Molecule Biophotonics lab at ICFO, Chris Burd, Ivan Castello-Serrano, and Ilya Levental for valuable discussions. We thank Nathalie Brouwers and the Centre for Genomic Regulation/Universitat Pompeu Fabra FACS Unit (Barcelona) for help with cell sorting and the IRB Barcelona Advanced Digital Microscopy (ADM) Core Facility for help with microscopy. We also thank Jordi Andilla and Maria Marsal for technical support

644 at the Super-resolution Light Nanoscopy (SLN) facility at ICFO. The authors acknowledge the
645 Protein Technologies Unit, Centre for Genomic Regulation (CRG) (Barcelona, Spain) for
646 providing the protein used in this study. C.G.-C. acknowledges a FPI fellowship awarded by
647 MINECO in the 2018 call. P.L., J.V.L., X.S., M.F.G.-P. and F.C. acknowledge support from
648 the Government of Spain (FIS2015-63550-R, BFU2015-73288-JIN, FIS2017-89560-R, RYC-
649 2017–22227, PID2019-106232RB-I00/10.13039/501100011033/110198RB-I00 and
650 PID2020-113068RB-I00 / 10.13039/501100011033; PID2022-138282NB-I00 project funded
651 by the MCIN/AEI/10.13039/501100011033/ FEDER, UE; and Severo Ochoa CEX2019-
652 000910-S), Fundació Privada Cellex, Fundació Privada Mir-Puig, and Generalitat de Catalunya
653 (CERCA, AGAUR), ERC Consolidator Grant CONCERT (GA 648201) and Advanced Grants
654 NANO-MEMEC (GA 788546) and LaserLab 4 Europe (GA 654148).

655

656 **AUTHOR CONTRIBUTIONS**

657 Conceptualization, P.L. and F.C.; Methodology, P.L., C.G.-C., Y.W., J. V. L., C.R., H.S., X.S.,
658 and F.C.; Software, C.R.; Formal analysis, P.L., C.G.-C., Y.W., C.R., X.S., V.M., M.F.G.-P.,
659 and F.C.; Investigation, P.L., C.G.-C., Y.W., J. V. L., C.R., H.S., and F.C.; Writing – Original
660 Draft, P.L. and F.C.; Writing – Review & Editing, all authors; Funding Acquisition, V.M., X.S.,
661 M.F.G.-P., and F.C.; Supervision, X.S., M.F.G.-P., and F.C.

662

663 **DECLARATION OF INTERESTS**

664 The authors declare no competing interests

665 **METHODS**

666 **Reagents and antibodies**

667 Brefeldin-A (BFA), from Sigma-Aldrich, was dissolved in Dimethyl Sulfoxide (DMSO)
668 (Sigma-Aldrich) as a 10 mg/mL stock solution, and used at 5 µg/ml concentration. N-
669 Hexanoyl-D-erythro-sphingosine (D-cer-C6), from Matreya, was dissolved in pure ethanol
670 (Merck) as a 10 mM stock solution, and used at 20 µM concentration. Cycloheximide was
671 purchased from A.G. Scientific, diluted to 1M in DMSO as a stock solution, and used at 100
672 µM concentration. Sheep anti-human TGN46 was from AbD Serotec. Mouse monoclonal
673 against HA was from Biolegend. Mouse monoclonal against Myc was from Sigma-Aldrich.
674 Rabbit polyclonal antibody against Flag was from Sigma-Aldrich. Rabbit polyclonal antibody
675 against GFP was from Abcam. Alexa Fluor-labeled secondary antibodies were from Invitrogen
676 and HRP-conjugated secondary antibodies from Sigma-Aldrich. For STORM, the

677 activator/reporter dye-conjugated secondary antibodies were in-house-labelled donkey-anti-
678 mouse and donkey-anti-rabbit obtained from ImmunoResearch, used at a final concentration of
679 20 µg/ml. The dyes used for labelling were NHS ester derivatives: Alexa Fluor 405 Carboxylic
680 Acid Succinimidyl Ester (Invitrogen), Cy3 mono-Reactive Dye Pack (GE HealthCare), and
681 Alexa Fluor 647 Carboxylic Acid succinimidyl Ester (Invitrogen). Antibody labelling reactions
682 were performed as previously reported (Borgman et al., 2020).

683 **Cell culture, plasmids and siRNA**

684 HeLa cells were cultured in DMEM (Lonza and Capricorn Scientific) containing 10% fetal
685 bovine serum (FBS) (ThermoFisher and Capricorn Scientific), 1% penicillin/streptomycin
686 (Biowest), and 2 mM L-Glutamine (Biowest). Cells were transfected with DNA using Xtreme-
687 GENE 9 DNA (Roche) or with TransIT-HeLaMonster (Mirus) following manufacturer's
688 recommendations. The TGN46-GFP plasmid, which was kindly provided by Dr. S.
689 Ponnambalam (Leeds University, Leeds, England, UK), was generated by inserting human
690 TGN46 cDNA into a pEGFP-N1 vector using the BamHI restriction site. TGN46 ΔAAIL-GFP,
691 TGN46-ST TMD-GFP, GFP-TGN46, GFP-TGN46 LT, GFP-TGN46 TC, GFP-TGN46lum,
692 GFP-TGN46lum-ST TMD, GFP-TGN46lum-ST TC, GFP-TGN46lum-VSVG TC, and GFP-
693 VSVG TC were sub-cloned by Gibson assembly (Gibson et al., 2009) and/or DNA digestion
694 and ligation using TGN46-GFP as a backbone and TGN46-GFP, ST-GFP, or VSVG-GFP as
695 DNA sequence providers. TGN46-mRFP was generated by Gibson assembly of the KpnI- and
696 EcoRI-digestion of the previously described plasmid PAUF-mRFP (Wakana et al., 2012).
697 TGN46-ST TMD-mCherry was sub-cloned by Gibson assembly using TGN46-mRFP as the
698 backbone and ST-GFP as DNA sequence providers. PAUF-MycHis and PAUF-mRFP
699 plasmids were described earlier (Wakana et al., 2012). ST-GFP, which encodes for the initial
700 45 amino acids of the ST6Gal-I ST, comprising the cytosolic domain, the TMD and 20 amino
701 acids of the lumenal domain, was cloned into pEGFP-N1 as previously described (Duran et al.,
702 2012). The ST-mCherry plasmid was generated from the previously described plasmid ST-
703 FKBP-mCherry (Pecot and Malhotra, 2004) by Gibson assembly of the BglII- and BamHI-
704 digested plasmid. The VSVG-GFP plasmid was described previously (von Blume et al., 2009).
705 VSVG-HA was generated by Gibson assembly from VSVG-GFP. PKD2-KD-Flag plasmid was
706 described earlier (Bossard et al., 2007). pETM14-6his-mGFP -TGN46lum plasmid for bacterial
707 expression was cloned using a synthetic fragment of bacterial optimized TGN46 (gblock IDT),
708 meGFP amplified from GFP-TGN46-lum and assembled in pETM14 backbone vector using
709 Gibson assembly. All plasmids were verified by sequencing (STAB vida). SnapGene software
710 (obtained from GSL Biotech) and ApE software (by M. Wayne Davis) were used for molecular
711 cloning procedures.

712 For TGN46 transient silencing, HeLa cells were transfected using HiPerFect Transfection
713 Reagent (QIAGEN) with 5 nM of TGN46 siRNA (oligo name: SASI_HS01_00080765, from
714 Sigma-Aldrich), following the manufacturer's recommendations. MISSION siRNA Universal
715 Negative Control #1 was used as a control siRNA. 48h after transfection, corresponding
716 experiments were performed.

717 Single-clone TGN46 KO HeLa cells were generated by CRISPR/Cas9. HeLa cells were
718 transfected with U6-gDNA (5'-AAAGACGTCCCTAACAAGT-3'; clone ID es:
719 HSPD0000063884): CMV-eCas9-2a-tGFP (Sigma-Aldrich). 48h after transfection, GFP-
720 positive cells were sorted as individual cells by FACS using a BD Influx cell sorter (BD
721 Biosciences). Upon clone expansion, KO effectiveness of the different clones was checked by
722 SDS-PAGE and Western blotting and also by immunofluorescence microscopy.

723 **Immunofluorescence microscopy**

724 Samples were fixed with 4% formaldehyde in PBS for 15 min and permeabilized and blocked
725 with 0.2% Triton X-100, 3% BSA in PBS for 30 min prior to antibody staining. Fixed samples
726 were analyzed with a TCS SP8 STED 3X system (Leica) in confocal mode using a 100x 1.4NA
727 objective and HyD detectors. Images were acquired using the Leica LAS X software and
728 converted to TIFF files using ImageJ (version 1.43; National Institutes of Health). Two-channel
729 colocalization analysis was performed using the ImageJ software and the Pearson's correlation
730 coefficient was calculated in a ROI using the "Manders Coefficients" plugin developed at the
731 Wright Cell Imaging Facility (Toronto, Canada). The ROI was determined as a mask created
732 on the Golgi region formed upon Binary transformation (using the Default Thresholding given
733 by the software) of the sum of both channels. Vesicle colocalization analysis was performed
734 using ImageJ and was calculated using the "Spots colocalization (ComDet)" plugin developed
735 by Eugene A. Katrukha (Utrecht University, Netherlands). Golgi-derived tubules were
736 quantified manually upon Z-projection (maximum intensity) performed using the ImageJ
737 software.

738 **FLIP microscopy**

739 Growth media of the HeLa cells seeded on Nunc Lab-Tek 8-wells 1.0 bottom glass chamber
740 slides was supplemented with 25 mM HEPES (pH 7.4) prior to experiment. FLIP experiment
741 was performed on a TCS STED CW system (Leica) in confocal mode using a 63x XNA
742 objective and HyD detectors. Using the Live Data Mode tool of Las AF software (Leica),
743 intermittent bleaching steps were combined with imaging of the whole cell during ~35 min.

744 When the FLIP experiments were performed on a GFP-containing protein, the series consisted
745 of the following steps: (1) Image 512x512 pixels and pixel size ~75 nm, 200 Hz acquisition

746 speed, 5% nominal power of an Argon Laser (488 nm). (2) Do 6x bleaching steps, keeping the
747 same parameters as in step 1, but with a 100% laser power on a manually selected region
748 encompassing the entire cell except the Golgi region. (3) Repeat step 1. (4) Pause for 40 s. (5)
749 Repeat step 1. (6) Repeat steps 2–5 for 35 times.

750 When the FLIP experiments were performed on a mRFP-containing protein, the series
751 consisted of the following steps: (1) Image 512x512 pixels and pixel size ~75 nm, 200 Hz
752 acquisition speed, 15% nominal power of a HeNe Laser (543 nm). (2) Do 5x bleaching steps,
753 keeping the same parameters as in step 1, but with a 100% laser power on a manually selected
754 region encompassing the entire cell except the Golgi region. (3) Repeat step 1. (4) Pause for 42
755 s. (5) Repeat step 1. (6) Repeat steps 2–5 for 35 times.

756 To measure Golgi export rate of the protein of interest, the mean intensity of the region left by
757 the photobleaching mask (Golgi-including region), $I(t)$, was measured over time and
758 normalized to the initial intensity, $I_0 = I(t = 0)$, using ImageJ and plotted using Prism 9.1.2
759 (GraphPad). Data was finally fitted to a one-phase decay curve fixing the "plateau" to 0, that is
760 $I(t)/I_0 = exp(-t/\tau)$, from where the half-life, $t_{1/2} = ln(2)\,\tau$, is extracted, and used to
761 compare the Golgi residence time among different proteins.

762 **STORM imaging and data analysis**

763 For STORM imaging, HeLa cells were cultured on 8-chambered glass bottom dishes
764 (Thermoscientific) at 37 °C with 5% CO_2. Plasmids containing the sequence of the gene of
765 interest were transfected and 24 hours after, cells were fixed with 4% paraformaldehyde in PBS
766 at room temperature for 15 minutes. After fixation, cells were washed, permeabilized with 0.1%
767 Triton X-100 (Fisher Scientific) (v/v) in PBS for 10 minutes, washed again, and blocked in 3%
768 BSA (Sigma Aldrich) (w/v) in PBS for 60 minutes. Then, cells were labeled with primary
769 antibodies, as detailed in the "Immunofluorescence microscopy" section. Donkey-anti-rabbit
770 conjugated with AF405/AF647 (3:1) and donkey-anti-mouse conjugated with Cy3/AF647 (7:1)
771 were used as secondary antibodies at 2 µg/mL final concentration.

772 STORM was performed in an imaging buffer containing 10 mM Cysteamine MEA
773 (SigmaAldrich), 0.5 mg/mL glucose oxidase (Sigma Aldrich), 40 µg/ml catalase (Sigma-
774 Aldrich), and 6.25% glucose (Sigma Aldrich) in PBS (Gómez-García et al., 2018). Two-colour
775 images were acquired on a commercial microscope system (Nikon Eclipse Ti N-STORM
776 system), from Nikon Instruments, equipped with a 100x oil objective with NA 1.49 using
777 oblique illumination. The detector was an ANDOR technology EMCCD iXon 897 camera, with
778 a 256x256 pixel ROI and a pixel size of 160 nm. Fluorophore excitation was done using an
779 Agilent technologies laser box with laser lines 405 nm, 561 nm, and 647 nm. NIS software

780 (Nikon) was used for acquiring the data. In a pre-acquisition step the sample was irradiated
781 with the 647 nm laser at 70% (~107 mW) power to bring a large majority of the dyes into a
782 dark (off) state. STORM acquisition was then performed sequentially using 20 ms frames by
783 maintaining the 647 nm laser at a constant power and using low power activator (405 nm or
784 561 nm) excitation (gradually increasing during acquisition from 0.5% to 100%). The
785 acquisitions were stopped after ~70,000 frames.

786 STORM image reconstruction was performed in Insight3 software (Huang et al., 2008). The
787 generated images were also corrected for cross-talked from images obtained from samples only
788 labelled with 1 pair of antibodies. For the image reconstruction, a list containing the localization
789 data for each channel were obtained. The degree of colocalization between both lists of
790 localization was measured within a Golgi- containing region of interest (ROI) using the Coloc-
791 Tesseler software (Levet et al., 2019). First, the software partition the image area into regions
792 per localization where any given point within that region will be closer to that localization than
793 to any other (Voronoi tessellation). Then, a first-rank density value, obtained from the area of
794 the neighbour Voronoi areas, is assigned for each localization. Subsequently, these first-rank
795 densities are represented in a logarithmic scaled scatterplot for each channel, always keeping
796 channel A in x-axis and channel B in y-axis. The values in the scatterplot for channel A (x^A,
797 y^A) correspond to the first-rank density of a localization in channel A (x^A) against the first-
798 rank density of the localization of channel B in whose Voronoi area the point in channel A
799 landed (y^A). Vice versa for the scatterplot associated to channel B.
800 Finally, the Spearman's rank correlation coefficients are quantified as a measure of the trength
801 and direction of the ranked variables plotted in each scatterplot. The Spearman's rank
802 correlation coefficient is defined as $S^A = 1 - \frac{6\sum_i\left(r(x_i^A)-r(y_i^A)\right)^2}{n_A({n_A}^2-1)}$, and $S^B = 1 -$
803 $\frac{6\sum_i\left(r(x_i^B)-r(y_i^B)\right)^2}{n_B({n_B}^2-1)}$, where $r\left(x_i^A\right)$ and $r\left(x_i^B\right)$ are the ranks of the first-rank density for channel A
804 in the scatterplots A and B respectively; $r\left(y_i^A\right)$ and $r\left(y_i^B\right)$ are the ranks of the first-rank density
805 of the channel B for the scatterplots A and B respectively; and n_A and n_B are the average
806 number of neighbours per channel. As the Pearson's correlation coefficient, the Spearman's
807 rank correlation coefficient varies from 1 (perfect localization) to -1 (perfect antilocalization)
808 and 0 representing a random distribution of localizations.

809 **Immunoprecipitation**

810 HeLa cells were lysed with lysis buffer (0.5% Triton X-100 in PBS) containing protease
811 inhibitors (Roche) for 15 min on ice, after which the samples were centrifuged at 16.000×g for
812 10 min at 4ºC. The resulting supernatants were incubated for 16 h while rotating at 4ºC with 8
813 µg/ml anti-GFP antibody (Roche). Protein A/G PLUS-Agarose (Santa Cruz) was then added to

814 the samples and incubated with rotation for 2 h at 4ºC. Immunoprecipitated fractions were
815 washed two times with lysis buffer and two more times with PBS, and heated to 95ºC for 5 min
816 with 1x Laemmli SDS sample buffer. The samples were subjected to SDS-PAGE and Western
817 blotting with anti-GFP (Santa Cruz) and anti-RFP (Abcam) antibodies.

818 **Secretion assay**

819 The growth media of HeLa WT and HeLa TGN46 KO cells seeded on a well of 6-wells plate -
820 and transfected with PAUF-Myc-His 48 h previous to the experiment performance- was
821 exchanged by pre-warmed (37ºC) DMEM containing 1% penicillin/streptomycin and 2 mM L-
822 Glutamine. Cells were then incubated for 4 h in an incubator at 37ºC and 5% CO_2 to collect
823 secreted PAUF-Myc-His protein. Then, media was collected in a 1.5 mL tube and centrifuged
824 to avoid floating dead cells that may interfere. Protease inhibitor was added to sample and
825 sample was concentrated down to 150 µL using Amicon Ultra-0.5 10 kDa Centrifugal Filter
826 Units (Merck). On the other hand, cells were lydes on ice with 150 uL of ice-cold lysis buffer
827 (1% SDS Tris-HCl pH 7.4). Samples were collected in a 1.5 mL tube using a scraper and
828 centrifuged at maximum speed for 20 min at 4ºC to remove cell pellet. Finally, 6x Laemmli
829 SDS sample buffer was added to both, supernatant and cell samples, and incubated for 10 min
830 at 95ºC. The samples were subjected to SDS-PAGE and Western blotting with anti-Myc (X)
831 and anti-TGN46 (AbD Serotec) antibodies. When cells were treated with BFA, the compound
832 was added to the cells to a final concentration of 5 µg/mL 15 min before media was exchanged
833 by FBS-deprived media and also to the collection media for the 4 h incubation time of the
834 secretion experiment.

835 **Statistics**

836 Statistical significance was tested using One-Way ANOVA using GraphPad Prism 9.1.2, unless
837 otherwise stated in the figure legend. Different data sets were considered to be statistically
838 significant when the p-value was ≤ 0.05 (*); p-value ≤ 0.01 (**); p-value ≤ 0.001 (***); p-value
839 ≤ 0.0001 (****).

840 **REFERENCES**

841 Banani, S.F., H.O. Lee, A.A. Hyman, and M.K. Rosen. 2017. Biomolecular condensates:
842 Organizers of cellular biochemistry. *Nat. Rev. Mol. Cell Biol.* 18:285–298.
843 doi:10.1038/nrm.2017.7.

844 Banfield, D.K. 2011. Mechanisms of protein retention in the Golgi. *Cold Spring Harb.*
845 *Perspect. Biol.* 3:1–14. doi:10.1101/cshperspect.a005264.

846 Banting, G., R. Maile, and E.P. Roquemore. 1998. The steady state distribution of
847 humTGN46 is not significantly altered in cells defective in clathrin-mediated
848 endocytosis. *J. Cell Sci.* 111:3451–3458. doi:10.1242/jcs.111.23.3451.

849 Banting, G., and S. Ponnambalam. 1997. TGN38 and its orthologues: Roles in post-TGN
850 vesicle formation and maintenance of TGN morphology. *Biochim. Biophys. Acta - Mol.*
851 *Cell Res.* 1355:209–217. doi:10.1016/S0167-4889(96)00146-2.

852 von Blume, J., A.M. Alleaume, G. Cantero-Recasens, A. Curwin, A. Carreras-Sureda, T.
853 Zimmermann, J. van Galen, Y. Wakana, M.A. Valverde, and V. Malhotra. 2011.
854 ADF/cofilin regulates secretory cargo sorting at the TGN via the Ca2+ ATPase SPCA1.
855 *Dev. Cell*. 20:652–662. doi:10.1016/j.devcel.2011.03.014.

856 von Blume, J., A.M. Alleaume, C. Kienzle, A. Carreras-Sureda, M. Valverde, and V.
857 Malhotra. 2012. Cab45 is required for Ca2+;-dependent secretory cargo sorting at the
858 trans-Golgi network. *J. Cell Biol.* 199:1057–1066. doi:10.1083/jcb.201207180.

859 von Blume, J., J.M. Duran, E. Forlanelli, A.M. Alleaume, M. Egorov, R. Polishchuk, H.
860 Molina, and V. Malhotra. 2009. Actin remodeling by ADF/cofilin is required for cargo
861 sorting at the trans-Golgi network. *J. Cell Biol.* 187:1055–1069.
862 doi:10.1083/jcb.200908040.

863 von Blume, J., and A. Hausser. 2019. Lipid-dependent coupling of secretory cargo sorting
864 and trafficking at the trans-Golgi network. *FEBS Lett.* 593:2412–2427.
865 doi:10.1002/1873-3468.13552.

866 Boncompain, G., and A. V. Weigel. 2018. Transport and sorting in the Golgi complex:
867 multiple mechanisms sort diverse cargo. *Curr. Opin. Cell Biol.* 50:94–101.
868 doi:10.1016/j.ceb.2018.03.002.

869 Borgman, K.J.E., G. Flórez-Grau, M.A. Ricci, C. Manzo, M. Lakadamyali, A. Cambi, D.
870 Benítez-Ribas, F. Campelo, and M.F. Garcia-Parajo. 2020. Membrane receptor MerTK
871 is a newly identified transcriptional regulator that associates to chromatin as

872 nanoclusters during human DC differentiation. *bioRxiv*. 2020.04.16.044974.
873 doi:10.1101/2020.04.16.044974.

874 Bos, K., C. Wraight, and K.K. Stanley. 1993. TGN38 is maintained in the trans-Golgi
875 network by a tyrosine-containing motif in the cytoplasmic domain. *EMBO J.* 12:2219–
876 2228. doi:10.1002/j.1460-2075.1993.tb05870.x.

877 Bossard, C., D. Bresson, R.S. Polishchuk, and V. Malhotra. 2007. Dimeric PKD regulates
878 membrane fission to form transport carriers at the TGN. *J. Cell Biol.* 179:1123–1131.
879 doi:10.1083/jcb.200703166.

880 Brangwynne, C.P., C.R. Eckmann, D.S. Courson, A. Rybarska, C. Hoege, J. Gharakhani, F.
881 Jülicher, and A.A. Hyman. 2009. Germline P granules are liquid droplets that localize
882 by controlled dissolution/condensation. *Science (80-.).* 324:1729–1732.
883 doi:10.1126/science.1172046.

884 Braulke, T., and J.S. Bonifacino. 2009. Sorting of lysosomal proteins. *Biochim. Biophys. Acta*
885 *- Mol. Cell Res.* 1793:605–614. doi:10.1016/j.bbamcr.2008.10.016.

886 Bretscher, M.S., and S. Munro. 1993. Cholesterol and the golgi apparatus. *Science (80-.).*
887 261:1280–1281. doi:10.1126/science.8362242.

888 Campelo, F., J. van Galen, G. Turacchio, S. Parashuraman, M.M. Kozlov, M.F. García-
889 Parajo, and V. Malhotra. 2017. Sphingomyelin metabolism controls the shape and
890 function of the golgi cisternae. *Elife*. 6. doi:10.7554/eLife.24603.

891 Cancino, J., J.E. Jung, and A. Luini. 2013. Regulation of Golgi signaling and trafficking by
892 the KDEL receptor. *Histochem. Cell Biol.* 140:395–405. doi:10.1007/s00418-013-1130-
893 9.

894 Capasso, S., L. Sticco, R. Rizzo, M. Pirozzi, D. Russo, N.A. Dathan, F. Campelo, J. Galen,
895 M. Hölttä-Vuori, G. Turacchio, A. Hausser, V. Malhotra, I. Riezman, H. Riezman, E.
896 Ikonen, C. Luberto, S. Parashuraman, A. Luini, and G. D'Angelo. 2017. Sphingolipid
897 metabolic flow controls phosphoinositide turnover at the trans -Golgi network . *EMBO*
898 *J.* 36:1736–1754. doi:10.15252/embj.201696048.

899 Case, L.B., J.A. Ditlev, and M.K. Rosen. 2019. Regulation of Transmembrane Signaling by
900 Phase Separation. *Annu. Rev. Biophys.* 48:465–494. doi:10.1146/annurev-biophys-
901 052118-115534.

902 Castello-Serrano, I., F.A. Heberle, B. Diaz-Rohrer, R. Ippolito, C.R. Shurer, P. Lujan, F.
903 Campelo, K.R. Levental, and I. Levental. 2023. Partitioning to ordered membrane

domains regulates the kinetics of secretory traffic. *Elife*. 12. doi:10.7554/ELIFE.89306.

Cosson, P., J. Perrin, and J.S. Bonifacino. 2013. Anchors aweigh: Protein localization and transport mediated by transmembrane domains. *Trends Cell Biol.* 23:511–517. doi:10.1016/j.tcb.2013.05.005.

Crevenna, A.H., B. Blank, A. Maiser, D. Emin, J. Prescher, G. Beck, C. Kienzle, K. Bartnik, B. Habermann, M. Pakde, H. Leonhardt, D.C. Lamb, and J. von Blume. 2016. Secretory cargo sorting by Ca2+-dependent Cab45 oligomerization at the trans-Golgi network. *J. Cell Biol.* 213:305–314. doi:10.1083/jcb.201601089.

Curwin, A.J., J. Von Blume, and V. Malhotra. 2012. Cofilin-mediated sorting and export of specific cargo from the Golgi apparatus in yeast. *Mol. Biol. Cell*. 23:2327–2338. doi:10.1091/mbc.E11-09-0826.

Deng, Y., M. Pakdel, B. Blank, E.L. Sundberg, C.G. Burd, and J. von Blume. 2018. Activity of the SPCA1 Calcium Pump Couples Sphingomyelin Synthesis to Sorting of Secretory Proteins in the Trans-Golgi Network. *Dev. Cell*. 47:464-478.e8. doi:10.1016/j.devcel.2018.10.012.

Deng, Y., F.E. Rivera-Molina, D.K. Toomre, and C.G. Burd. 2016. Sphingomyelin is sorted at the trans Golgi network into a distinct class of secretory vesicle. *Proc. Natl. Acad. Sci. U. S. A.* 113:6677–6682. doi:10.1073/pnas.1602875113.

Diaz-Rohrer, B.B., K.R. Levental, K. Simons, and I. Levental. 2014. Membrane raft association is a determinant of plasma membrane localization. *Proc. Natl. Acad. Sci. U. S. A.* 111:8500–8505. doi:10.1073/pnas.1404582111.

Dmitrieff, S., M. Rao, and P. Sens. 2013. Quantitative analysis of intra-Golgi transport shows intercisternal exchange for all cargo. *Proc. Natl. Acad. Sci. U. S. A.* 110:15692–15697. doi:10.1073/pnas.1303358110.

Dunn, K.W., M.M. Kamocka, and J.H. McDonald. 2011. A practical guide to evaluating colocalization in biological microscopy. *Am. J. Physiol. - Cell Physiol.* 300:C723. doi:10.1152/ajpcell.00462.2010.

Duran, J.M., F. Campelo, J. Van Galen, T. Sachsenheimer, J. Sot, M. V. Egorov, C. Rentero, C. Enrich, R.S. Polishchuk, F.M. Goñi, B. Brügger, F. Wieland, and V. Malhotra. 2012. Sphingomyelin organization is required for vesicle biogenesis at the Golgi complex. *EMBO J.* 31:4535–4546. doi:10.1038/emboj.2012.317.

Ford, C., A. Parchure, J. von Blume, and C.G. Burd. 2021. Cargo sorting at the trans-Golgi

network at a glance. *J. Cell Sci.* 134. doi:10.1242/jcs.259110.

van Galen, J., F. Campelo, E. Martínez-Alonso, M. Scarpa, J.Á. Martínez-Menárguez, and V. Malhotra. 2014. Sphingomyelin homeostasis is required to form functional enzymatic domains at the trans-Golgi network. *J. Cell Biol.* 206:609–618. doi:10.1083/jcb.201405009.

Garcia-Cabau, C., and X. Salvatella. 2021. Regulation of biomolecular condensate dynamics by signaling. *Curr. Opin. Cell Biol.* 69:111–119. doi:10.1016/j.ceb.2021.01.002.

Gibson, D.G., L. Young, R.Y. Chuang, J.C. Venter, C.A. Hutchison 3rd, and H.O. Smith. 2009. Enzymatic assembly of DNA molecules up to several hundred kilobases. *Nat Methods*. 6:343–345. doi:10.1038/nmeth.1318.

Gómez-García, P.A., E.T. Garbacik, J.J. Otterstrom, M.F. Garcia-Parajo, and M. Lakadamyali. 2018. Excitation-multiplexed multicolor superresolution imaging with fm-STORM and fm-DNA-PAINT. *Proc. Natl. Acad. Sci. U. S. A.* 115:12991–12996. doi:10.1073/pnas.1804725115.

Guo, Y., D.W. Sirkis, and R. Schekman. 2014. Protein sorting at the trans-Golgi network. *Annu. Rev. Cell Dev. Biol.* 30:169–206. doi:10.1146/annurev-cellbio-100913-013012.

Hirschberg, K., C.M. Miller, J. Ellenberg, J.F. Presley, E.D. Siggia, R.D. Phair, and J. Lippincott-Schwartz. 1998. Kinetic analysis of secretory protein traffic and characterization of Golgi to plasma membrane transport intermediates in living cells. *J. Cell Biol.* 143:1485–1503. doi:10.1083/jcb.143.6.1485.

Huang, B., W. Wang, M. Bates, and X. Zhuang. 2008. Three-dimensional super-resolution imaging by stochastic optical reconstruction microscopy. *Science (80-.).* 319:810–813. doi:10.1126/science.1153529.

Huet-Calderwood, C., F. Rivera-Molina, D. V. Iwamoto, E.B. Kromann, D. Toomre, and D.A. Calderwood. 2017. Novel ecto-tagged integrins reveal their trafficking in live cells. *Nat. Commun.* 8:1–13. doi:10.1038/s41467-017-00646-w.

Humphrey, J.S., P.J. Peters, L.C. Yuan, and J.S. Bonifacino. 1993. Localization of TGN38 to the trans-Golgi network: Involvement of a cytoplasmic tyrosine-containing sequence. *J. Cell Biol.* 120:1123–1136. doi:10.1083/jcb.120.5.1123.

Hyman, A.A., C.A. Weber, and F. Jülicher. 2014. Liquid-liquid phase separation in biology. *Annu. Rev. Cell Dev. Biol.* 30:39–58. doi:10.1146/annurev-cellbio-100913-013325.

Ishikawa-Ankerhold, H.C., R. Ankerhold, and G.P.C. Drummen. 2012. Advanced

968 Fluorescence Microscopy Techniques—FRAP, FLIP, FLAP, FRET and FLIM. *Mol.*
969 *2012, Vol. 17, Pages 4047-4132*. 17:4047–4132. doi:10.3390/MOLECULES17044047.

970 Jones, S.M., J.R. Crosby, J. Salamero, and K.E. Howell. 1993. A cytosolic complex of p62
971 and rab6 associates with TGN38/41 and is involved in budding of exocytic vesicles
972 from the trans-Golgi network. *J. Cell Biol.* 122:775–788. doi:10.1083/jcb.122.4.775.

973 Kienzle, C., N. Basnet, A.H. Crevenna, G. Beck, B. Habermann, N. Mizuno, and J. von
974 Blume. 2014. Cofilin recruits F-actin to SPCA1 and promotes Ca2+-mediated secretory
975 cargo sorting. *J. Cell Biol.* 206:635–654. doi:10.1083/jcb.201311052.

976 Kienzle, C., and J. von Blume. 2014. Secretory cargo sorting at the trans-Golgi network.
977 *Trends Cell Biol.* 24:584–593. doi:10.1016/j.tcb.2014.04.007.

978 Kulak, N.A., G. Pichler, I. Paron, N. Nagaraj, and M. Mann. 2014. Minimal, encapsulated
979 proteomic-sample processing applied to copy-number estimation in eukaryotic cells.
980 *Nat. Methods*. 11:319–324. doi:10.1038/nmeth.2834.

981 Lee, S.S., and G. Banting. 2002. Characterisation of the lumenal domain of TGN38 and
982 effects of elevated expression of TGN38 on glycoprotein secretion. *Eur. J. Cell Biol.*
983 81:609–621. doi:10.1078/0171-9335-00279.

984 Levet, F., G. Julien, R. Galland, C. Butler, A. Beghin, A. Chazeau, P. Hoess, J. Ries, G.
985 Giannone, and J.B. Sibarita. 2019. A tessellation-based colocalization analysis approach
986 for single-molecule localization microscopy. *Nat. Commun.* 10:1–12.
987 doi:10.1038/s41467-019-10007-4.

988 Liljedahl, M., Y. Maeda, A. Colanzi, I. Ayala, J. Van Lint, and V. Malhotra. 2001. Protein
989 Kinase D regulates the fission of cell surface destined transport carriers from the trans-
990 Golgi network. *Cell*. 104:409–420. doi:10.1016/S0092-8674(01)00228-8.

991 Lippincott-Schwartz, J., and R.D. Phair. 2010. Lipids and cholesterol as regulators of traffic
992 in the endomembrane system. *Annu. Rev. Biophys.* 39:559–578.
993 doi:10.1146/annurev.biophys.093008.131357.

994 Lorent, J.H., B. Diaz-Rohrer, X. Lin, K. Spring, A.A. Gorfe, K.R. Levental, and I. Levental.
995 2017. Structural determinants and functional consequences of protein affinity for
996 membrane rafts. *Nat. Commun.* 8. doi:10.1038/s41467-017-01328-3.

997 Luini, A., and S. Parashuraman. 2016. Signaling at the Golgi: Sensing and controlling the
998 membrane fluxes. *Curr. Opin. Cell Biol.* 39:37–42. doi:10.1016/j.ceb.2016.01.014.

999 Lujan, P., J. Angulo-Capel, M. Chabanon, and F. Campelo. 2021. Interorganelle

1000 communication and membrane shaping in the early secretory pathway. *Curr. Opin. Cell*
1001 *Biol.* 71:95–102. doi:10.1016/j.ceb.2021.01.010.

1002 Lujan, P., and F. Campelo. 2021. Should I stay or should I go? Golgi membrane spatial
1003 organization for protein sorting and retention. *Arch. Biochem. Biophys.* 707:108921.
1004 doi:10.1016/j.abb.2021.108921.

1005 Luzio, J.P., B. Brake, G. Banting, K.E. Howell, P. Braghetta, and K.K. Stanley. 1990.
1006 Identification, sequencing and expression of an integral membrane protein of the trans-
1007 Golgi network (TGN38). *Biochem. J.* 270:97–102. doi:10.1042/bj2700097.

1008 Malhotra, V., and F. Campelo. 2011. PKD regulates membrane fission to generate TGN to
1009 cell surface transport carriers. *Cold Spring Harb. Perspect. Biol.* 3:1–9.
1010 doi:10.1101/cshperspect.a005280.

1011 Mallet, W.G., and F.R. Maxfield. 1999. Chimeric forms of furin and TGN38 are transported
1012 from the plasma membrane to the trans-Golgi network via distinct endosomal pathways.
1013 *J. Cell Biol.* 146:345–359. doi:10.1083/jcb.146.2.345.

1014 Di Martino, R., L. Sticco, and A. Luini. 2019. Regulation of cargo export and sorting at the
1015 trans-Golgi network. *FEBS Lett.* 593:2306–2318. doi:10.1002/1873-3468.13572.

1016 McNamara, J.O., J.C. Grigston, H.M.A. VanDongen, and A.M.J. VanDongen. 2004. Rapid
1017 dendritic transport of TGN38, a putative cargo receptor. *Mol. Brain Res.* 127:68–78.
1018 doi:10.1016/j.molbrainres.2004.05.013.

1019 Van Meer, G., D.R. Voelker, and G.W. Feigenson. 2008. Membrane lipids: Where they are
1020 and how they behave. *Nat. Rev. Mol. Cell Biol.* 9:112–124. doi:10.1038/nrm2330.

1021 Milovanovic, D., A. Honigmann, S. Koike, F. Göttfert, G. Pähler, M. Junius, S. Müllar, U.
1022 DIederichsen, A. Janshoff, H. Grubmüller, H.J. Risselada, C. Eggeling, S.W. Hell, G.
1023 Van Den Bogaart, and R. Jahn. 2015. Hydrophobic mismatch sorts SNARE proteins
1024 into distinct membrane domains. *Nat. Commun.* 6:5984. doi:10.1038/ncomms6984.

1025 Mitra, K., I. Ubarretxena-Belandia, T. Taguchi, G. Warren, and D.M. Engelman. 2004.
1026 Modulation of the bilayer thickness of exocytic pathway membranes by membrane
1027 proteins rather than cholesterol. *Proc. Natl. Acad. Sci. U. S. A.* 101:4083–4088.
1028 doi:10.1073/pnas.0307332101.

1029 Mittag, T., and R. V. Pappu. 2022. A conceptual framework for understanding phase
1030 separation and addressing open questions and challenges. *Mol. Cell*. 82:2201–2214.
1031 doi:10.1016/J.MOLCEL.2022.05.018.

1032 Munro, S. 1991. Sequences within and adjacent to the transmembrane segment of α-2, 6-
1033 sialyltransferase specify Golgi retention. *EMBO J.* 10:3577–3588. doi:10.1002/j.1460-
1034 2075.1991.tb04924.x.

1035 Munro, S. 1995. An investigation of the role of transmembrane domains in Golgi protein
1036 retention. *EMBO J.* 14:4695–4704. doi:10.1002/j.1460-2075.1995.tb00151.x.

1037 Ohno, H., M.C. Fournier, G. Poy, and J.S. Bonifacino. 1996. Structural determinants of
1038 interaction of tyrosine-based sorting signals with the adaptor medium chains. *J. Biol.*
1039 *Chem.* 271:29009–29015. doi:10.1074/jbc.271.46.29009.

1040 Parchure, A., M. Tian, D. Stalder, C.K. Boyer, S.C. Bearrows, K.E. Rohli, J. Zhang, F.
1041 Rivera-Molina, B.R. Ramazanov, S.K. Mahata, Y. Wang, S.B. Stephens, D.C.
1042 Gershlick, and J. von Blume. 2022. Liquid–liquid phase separation facilitates the
1043 biogenesis of secretory storage granules. *J. Cell Biol.* 221. doi:10.1083/jcb.202206132.

1044 Patterson, G.H., K. Hirschberg, R.S. Polishchuk, D. Gerlich, R.D. Phair, and J. Lippincott-
1045 Schwartz. 2008. Transport through the Golgi Apparatus by Rapid Partitioning within a
1046 Two-Phase Membrane System. *Cell*. 133:1055–1067. doi:10.1016/j.cell.2008.04.044.

1047 Pecot, M.Y., and V. Malhotra. 2004. Golgi membranes remain segregated from the
1048 endoplasmic reticulum during mitosis in mammalian cells. *Cell*. 116:99–107.

1049 Ponnambalam, S., M. Girotti, M.L. Yaspo, C.E. Owen, A.C.F. Perry, T. Suganuma, T.
1050 Nilsson, M. Fried, G. Banting, and G. Warren. 1996. Primate homologues of rat
1051 TGN38: Primary structure, expression and functional implications. *J. Cell Sci.* 109:675–
1052 685. doi:10.1242/jcs.109.3.675.

1053 Quiroga, R., A. Trenchi, A.G. Montoro, J.V. Taubas, and H.J.F. Maccioni. 2013. Short
1054 transmembrane domains with high-volume exoplasmic halves determine retention of
1055 type II membrane proteins in the golgi complex. *J. Cell Sci.* 126:5344–5349.
1056 doi:10.1242/jcs.130658.

1057 Rajasekaran, A.K., J.S. Humphrey, M. Wagner, G. Miesenböck, A. Le Bivic, J.S. Bonifacino,
1058 and E. Rodriguez-Boulan. 1994. TGN38 recycles basolaterally in polarized Madin-
1059 Darby canine kidney cells. *Mol. Biol. Cell*. 5:1093–1103. doi:10.1091/mbc.5.10.1093.

1060 Ramazanov, B.R., M.L. Tran, and J. von Blume. 2021. Sending out molecules from the TGN.
1061 *Curr. Opin. Cell Biol.* 71:55–62. doi:10.1016/j.ceb.2021.02.005.

1062 Reaves, B., M. Horn, and G. Banting. 1993. TGN38/41 recycles between the cell surface and
1063 the TGN: Brefeldin A affects its rate of return to the TGN. *Mol. Biol. Cell*. 4:93–105.

1064 doi:10.1091/mbc.4.1.93.

1065 Sharpe, H.J., T.J. Stevens, and S. Munro. 2010. A Comprehensive Comparison of
1066 Transmembrane Domains Reveals Organelle-Specific Properties. *Cell*. 142:158–169.
1067 doi:10.1016/j.cell.2010.05.037.

1068 Shin, Y., and C.P. Brangwynne. 2017. Liquid phase condensation in cell physiology and
1069 disease. *Science (80-.).* 357. doi:10.1126/science.aaf4382.

1070 Spang, A. 2015. The road not taken: Less traveled roads from the TGN to the plasma
1071 membrane. *Membranes (Basel).* 5:84–98. doi:10.3390/membranes5010084.

1072 Stalder, D., and D.C. Gershlick. 2020. Direct trafficking pathways from the Golgi apparatus
1073 to the plasma membrane. *Semin. Cell Dev. Biol.* 107:112–125.
1074 doi:10.1016/j.semcdb.2020.04.001.

1075 Stanley, K.K., and K.E. Howell. 1993. TGN38/41: a molecule on the move. *Trends Cell Biol.*
1076 3:252–255. doi:10.1016/0962-8924(93)90046-4.

1077 Tie, H.C., D. Mahajan, and L. Lu. 2022. Visualizing intra-Golgi localization and transport by
1078 side-averaging Golgi ministacks. *J. Cell Biol.* 221. doi:10.1083/jcb.202109114.

1079 Tu, L., W.C.S. Tai, L. Chen, and D.K. Banfield. 2008. Signal-mediated dynamic retention of
1080 glycosyltransferases in the Golgi. *Science (80-.).* 321:404–407.
1081 doi:10.1126/science.1159411.

1082 Wakana, Y., and F. Campelo. 2021. The PKD-dependent biogenesis of TGN-to-plasma
1083 membrane transport carriers. *Cells*. 10:1618. doi:10.3390/cells10071618.

1084 Wakana, Y., J. Van Galen, F. Meissner, M. Scarpa, R.S. Polishchuk, M. Mann, and V.
1085 Malhotra. 2012. A new class of carriers that transport selective cargo from the trans
1086 Golgi network to the cell surface. *EMBO J.* 31:3976–3990.
1087 doi:10.1038/emboj.2012.235.

1088 Wakana, Y., K. Hayashi, T. Nemoto, C. Watanabe, M. Taoka, J. Angulo-Capel, M.F. Garcia-
1089 Parajo, H. Kumata, T. Umemura, H. Inoue, K. Arasaki, F. Campelo, and M. Tagaya.
1090 2021. The ER cholesterol sensor SCAP promotes CARTS biogenesis at ER–golgi
1091 membrane contact sites. *J. Cell Biol.* 220. doi:10.1083/jcb.202002150.

1092 Wakana, Y., R. Kotake, N. Oyama, M. Murate, T. Kobayashi, K. Arasaki, H. Inoue, and M.
1093 Tagaya. 2015. CARTS biogenesis requires VAP-lipid transfer protein complexes
1094 functioning at the endoplasmic reticulum-Golgi interface. *Mol. Biol. Cell*. 26:4686–
1095 4699. doi:10.1091/mbc.E15-08-0599.

1096 Wakana, Y., J. Villeneuve, J. van Galen, D. Cruz-Garcia, M. Tagaya, and V. Malhotra. 2013.
1097 Kinesin-5/Eg5 is important for transport of CARTS from the trans-Golgi network to the
1098 cell surface. *J. Cell Biol.* 202:241–250. doi:10.1083/jcb.201303163.

1099 Wang, J., and K.E. Howell. 2000. The luminal domain of TGN38 interacts with integrin β1
1100 and is involved in its trafficking. *Traffic*. 1:713–723. doi:10.1034/j.1600-
1101 0854.2000.010904.x.

1102 Wang, J., M.S. Ladinsky, and K.E. Howell. 1995. Molecules and vesicle coats involved in the
1103 budding of exocytotic vesicles from the trans-Golgi network. *Cold Spring Harb. Symp.*
1104 *Quant. Biol.* 60:139–146. doi:10.1101/SQB.1995.060.01.017.

1105 Welch, L.G., and S. Munro. 2019. A tale of short tails, through thick and thin: investigating
1106 the sorting mechanisms of Golgi enzymes. *FEBS Lett.* 593:2452–2465.
1107 doi:10.1002/1873-3468.13553.

1108 Welch, L.G., S.Y. Peak-Chew, F. Begum, T.J. Stevens, and S. Munro. 2021. Golph3 and
1109 golph3l are broad-spectrum copi adaptors for sorting into intra-golgi transport vesicles.
1110 *J. Cell Biol.* 220. doi:10.1083/jcb.202106115.

1111 Wood, C.S., K.R. Schmitz, N.J. Bessman, T.G. Setty, K.M. Ferguson, and C.G. Burd. 2009.
1112 PtdIns4P recognition by Vps74/GOLPH3 links PtdIns 4-kinase signaling to retrograde
1113 Golgi trafficking. *J. Cell Biol.* 187:967–975. doi:10.1083/jcb.200909063.

1114 Yeaman, C., M.I. Ayala, J.R. Wright, F. Bard, C. Bossard, A. Ang, Y. Maeda, T. Seufferlein,
1115 I. Mellman, W.J. Nelson, and V. Malhotra. 2004. Protein kinase D regulates basolateral
1116 membrane protein exit from trans-Golgi network. *Nat. Cell Biol.* 6:106–112.
1117 doi:10.1038/ncb1090.

1118 Zappa, F., M. Failli, and M.A. De Matteis. 2018. The Golgi complex in disease and therapy.
1119 *Curr. Opin. Cell Biol.* 50:102–116. doi:10.1016/j.ceb.2018.03.005.

1120 Zhang, J., A. Kennedy, L. Xing, S. Bui, W. Reid, J. Joppich, E. Ahat, M. Rose, Q. Tang,
1121 A.W. Tai, and Y. Wang. 2022. SARS-CoV-2 triggers Golgi fragmentation via down-
1122 regulation of GRASP55 to facilitate viral trafficking. *bioRxiv Prepr. Serv. Biol.*
1123 2022.03.04.483074. doi:10.1101/2022.03.04.483074.

1124

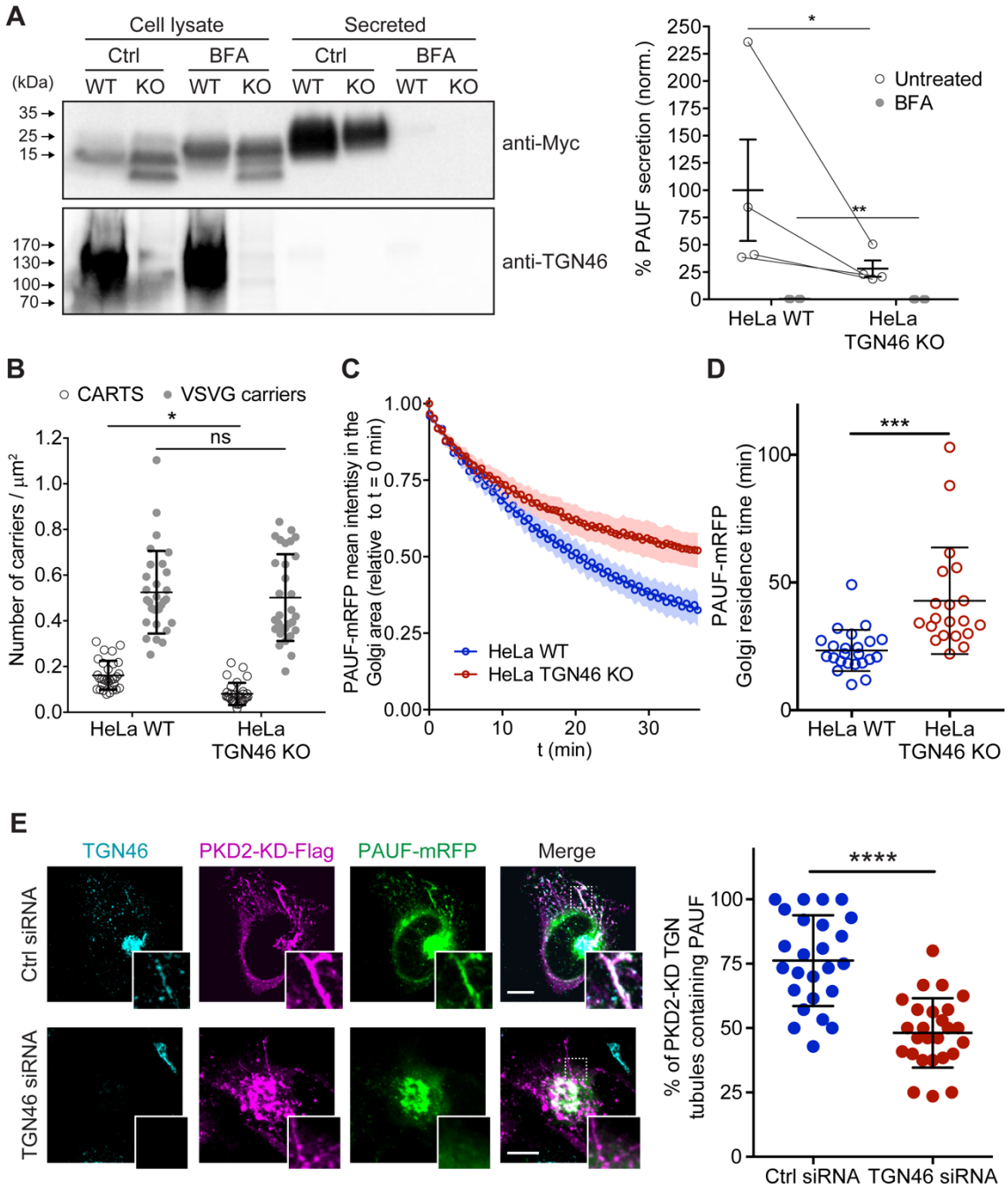

Figure 1. TGN46 is required for cargo sorting and loading into CARTS. (A) PAUF secretion assay in parental (WT) and CRISPR/Cas9-mediated TGN46 knockout (KO) HeLa cells. Cells expressing PAUF-MycHis were incubated for 4 h in fresh medium without serum in the absence (Ctrl) or presence of Brefeldin A (BFA), after which the cells were lysed. Equal amounts of cell lysates and their corresponding secreted fraction (medium) were analyzed by western blotting (left) using an anti-Myc antibody (top blot) and anti-TGN46 antibody (bottom blot). BFA was included as a positive control of secretion inhibition. Quantification (right) of the ratio of secreted/internal PAUF signal normalized (norm.) as a percentage to the average value of the WT, Ctrl condition. n=4 independent experiments. Individual values shown with connecting lines between paired data sets (shown only for untreated condition, for clarity), with mean ± stdev. Paired t test (*, $p \leq 0.05$). **(B)** Number of carriers (CARTS, empty circles; VSVG carriers, gray circles) per unit area observed in WT or TGN46-KO HeLa cells expressing either PAUF-mRFP (CARTS marker) and VSVG-HA (VSVG carrier marker). At least 10 cells from each of n=3 independent experiments were quantified. Individual values shown, with mean ± stdev. Unpaired two-tailed t test (ns, $p > 0.05$; *, $p \leq 0.05$). **(C)** Relative fluorescence intensity average time trace (mean ± s.e.m.) of FLIP experiments performed in WT or TGN46-KO HeLa cells expressing PAUF-mRFP. **(D)** Quantification of the PAUF-mRFP Golgi residence time as obtained from the FLIP experiments, as the one shown in **(C)**. Between 7–12 cells from each of n=3 independent experiments were quantified. Individual values shown, with mean ± stdev. Unpaired two-tailed t test (***, $p \leq 0.001$). **(E)** Left panels are confocal fluorescence microscopy images of HeLa cells transfected with control (Ctrl) or TGN46 siRNA, which were also transfected with PKD2-KD-Flag and PAUF-mRFP. Cells were fixed at steady state and labelled with anti-TGN46 (cyan) and anti-Flag (magenta) antibodies. PAUF-

mRFP fluorescence signal is shown in green. Scale bars are 10 µm, magnifications of the boxed regions are shown. In the right panel, the quantification of the percentage of PKD2-KD-induced tubules that containing PAUF-mRFP in control (Ctrl) or TGN46 siRNA-treated cells. At least 10 cells from each of n=3 independent experiments. Individual values shown, with mean ± stdev. Unpaired two-tailed t test (****, $p \leq 0.0001$).

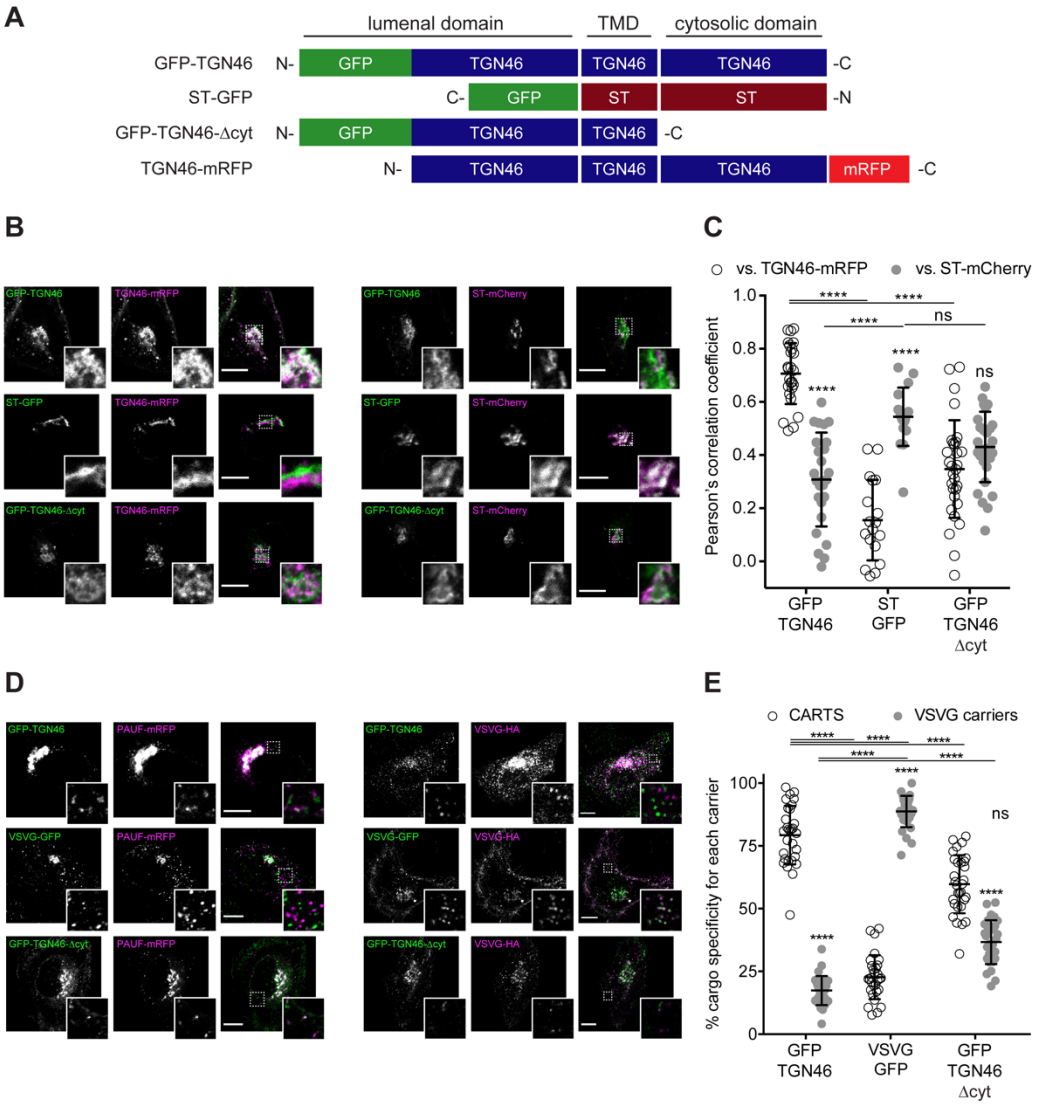

Figure 2. TGN46 export in CARTS is not dependent on cytosolic tail signals. (A) Schematic representation of construct domain topology. Notice that type I proteins (e.g., GFP-TGN46) have a lumenal N-terminal domain, whereas type II proteins (e.g., ST-GFP) have a cytosolic N-terminal domain. TMD: transmembrane domain. **(B)** HeLa cells co-expressing the different indicated proteins (green and magenta channels) were fixed, and the localization of those proteins was monitored by fluorescence confocal microscopy. Insets correspond to zoom-in areas of the dashed, white boxed areas. **(C)** Pearson's correlation coefficient between the perinuclear fluorescence signal of the x-axis indicated proteins with respect to TGN46-mRFP (empty circles) or ST-mCherry (gray circles), measured from confocal micrographs in **(B)**. Results are from at least 10 cells from each of n=3 independent experiments (individual values shown, with mean ± stdev). **(D)** HeLa cells co-expressing the different indicated proteins (green and magenta channels) were fixed, processed for immunostaining when required, and the localization of those proteins was monitored by fluorescence confocal microscopy. Insets correspond to zoom-in areas of the dashed, white boxed areas. **(E)** Percentage of transport carriers containing each of the cargoes described on the x-axis that are also positive for PAUF (CARTS, empty circles) or VSVG (VSVG carriers, gray circles), as measured from confocal micrographs in **(D)**. Results are from at least 10 cells from each of n=3 independent experiments (individual values shown, with mean ± stdev). Scale bars in **(B, D)** are 10 µm.

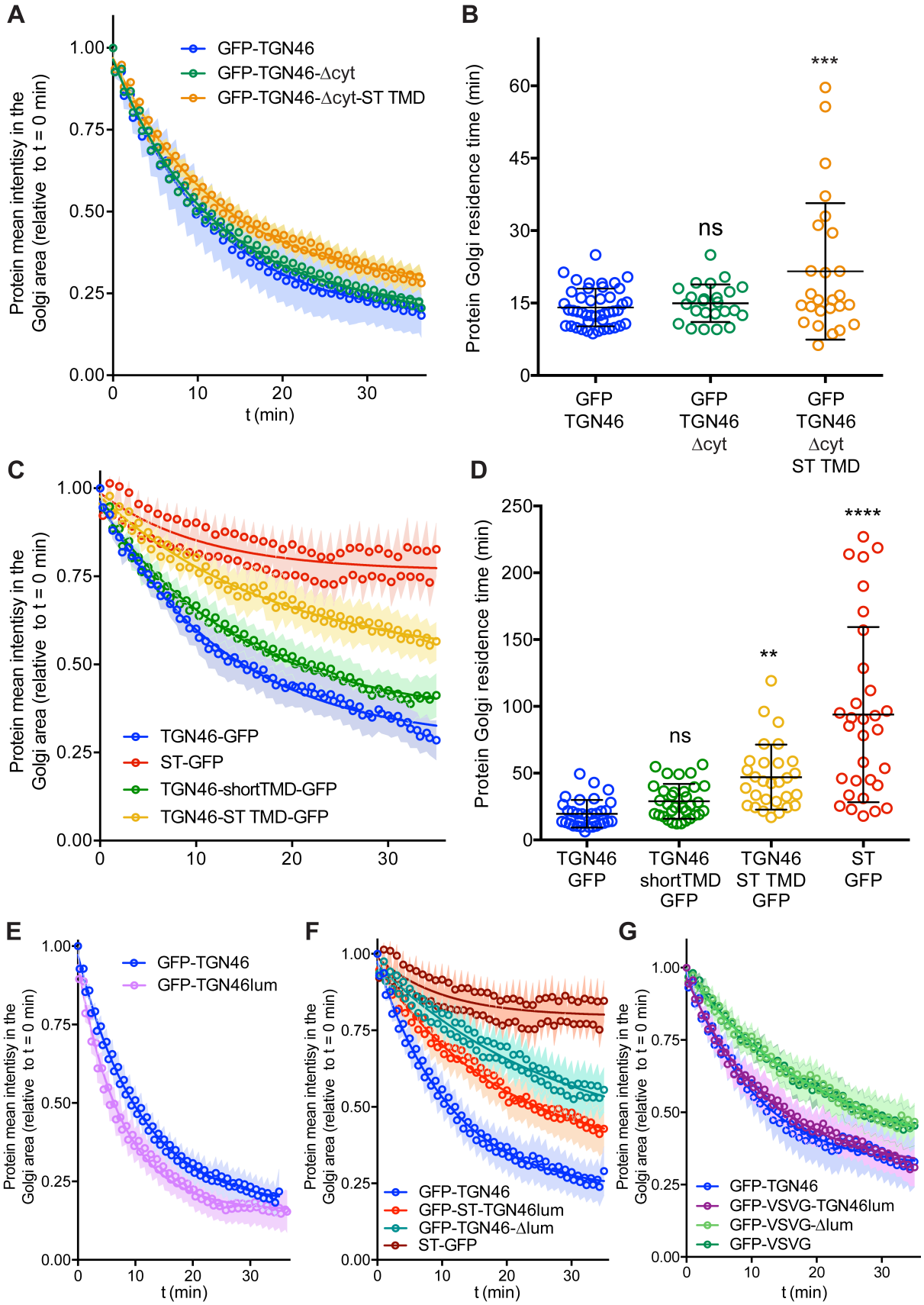

Figure 3. FLIP experiments monitor Golgi residence times of different proteins. (A, C, E–G) Relative fluorescence intensity average time trace (mean ± s.e.m.) of FLIP experiments for the indicated proteins. Symbols correspond to actual measurements, solid lines to the fitted exponential decays. **(B, D)** Residence time in the perinuclear area measured as the half time of the FLIP curves. Results are from 7–12 cells from each of n=3 independent experiments (individual values shown, with mean ± stdev).

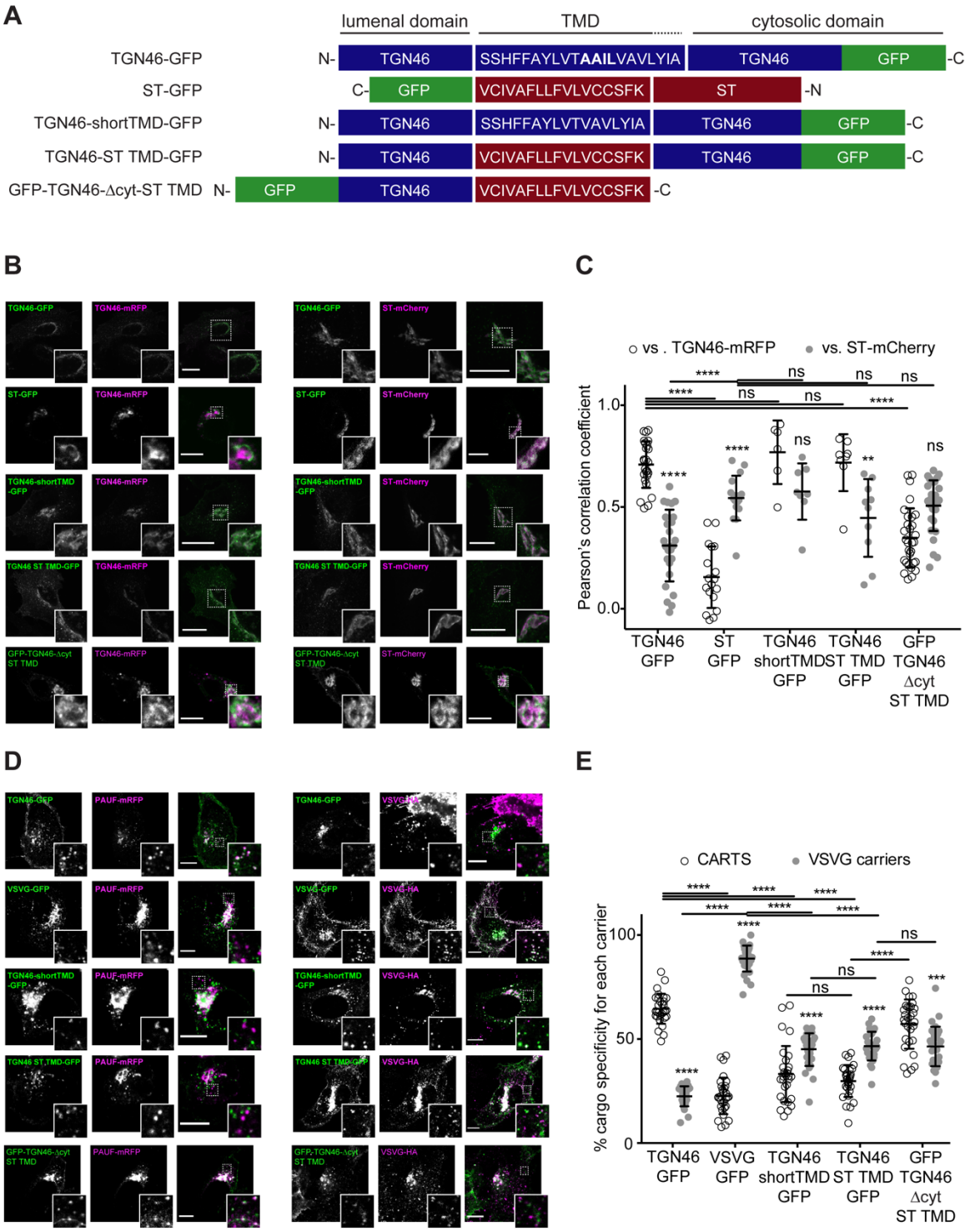

Figure 4. TGN46 intra-Golgi localization and CARTS specificity are insensitive to TMD length and composition. (A) Schematic representation of construct domain topology. The amino acid sequence (in the correct topology) of the different transmembrane domains (TMD) is indicated. **(B)** HeLa cells co-expressing the different indicated proteins (green and magenta channels) were fixed, and the localization of those proteins was monitored by fluorescence confocal microscopy. Insets correspond to zoom-in areas of the dashed, white boxed areas. **(C)** Pearson's correlation coefficient between the perinuclear fluorescence signal of the x-axis indicated proteins with respect to TGN46-mRFP (empty circles) or ST-mCherry (gray circles), measured from confocal micrographs in **(B)**. Results are at least 3 cells from each of n=3 independent experiments (individual values shown, with mean ± stdev). **(D)** HeLa cells co-expressing the different indicated proteins (green and magenta channels) were fixed, processed for immunostaining when required, and the localization of those proteins was monitored by fluorescence confocal microscopy. Insets correspond to zoom-in areas of the dashed, white boxed areas. **(E)** Percentage of transport carriers containing each of the cargoes described on the x-axis that are also positive for PAUF (CARTS, empty circles) or VSVG (VSVG carriers, gray circles), as measured from confocal micrographs in **(D)**. Results are from at least 10 cells from each of n=3 independent experiments (individual values shown, with mean ± stdev). Scale bars in **(B, D)** are 10 µm.

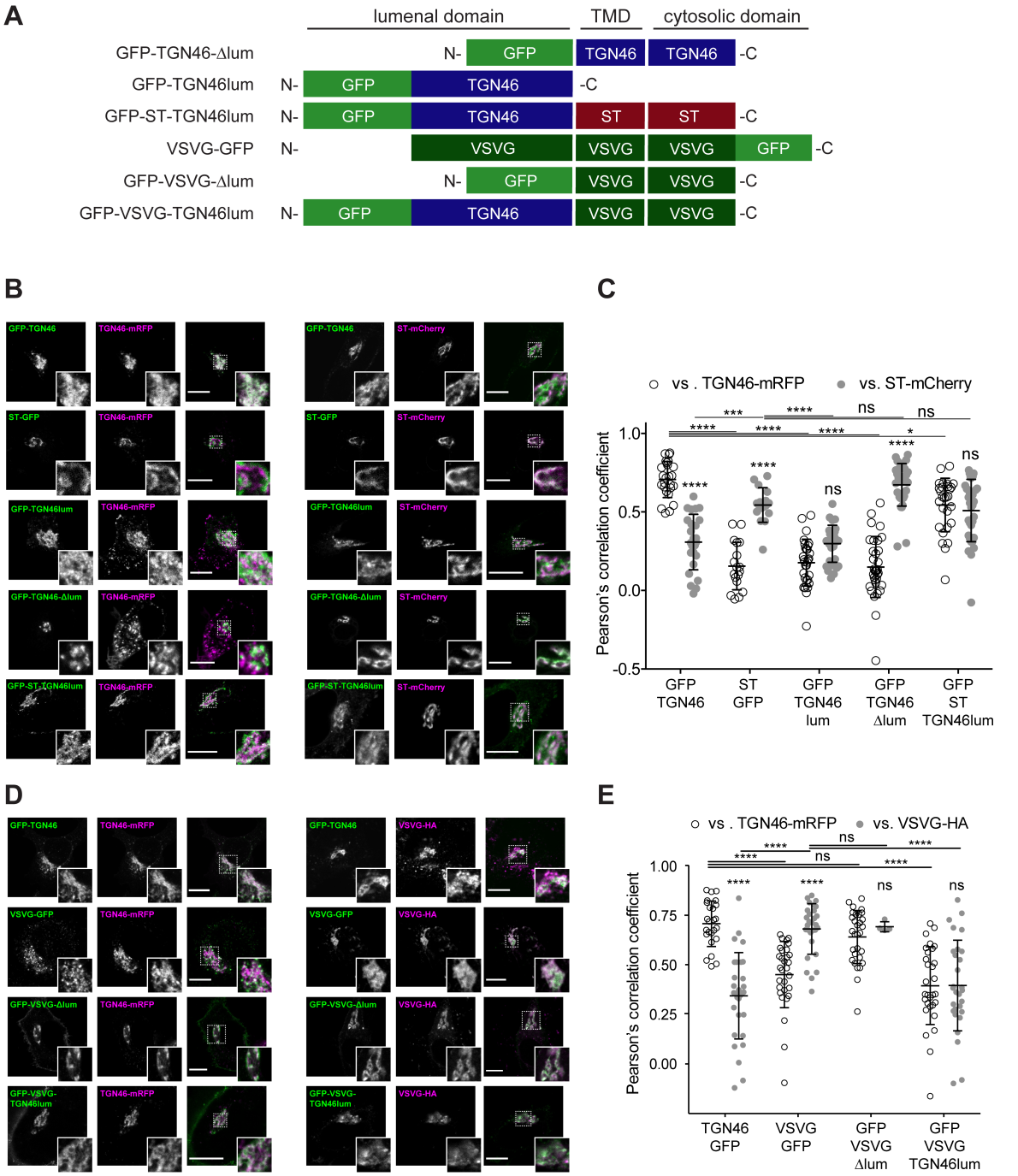

Figure 5. Intra-Golgi localization analysis for the role of the lumenal domain of TGN46 in CARTS-mediated export from the TGN. (A) Schematic representation of construct domain topology. TMD: transmembrane domain. **(B)** HeLa cells co-expressing the different indicated proteins (green and magenta channels) were fixed, and the localization of those proteins was monitored by fluorescence confocal microscopy. Insets correspond to zoom-in areas of the dashed, white boxed areas. **(C)** Pearson's correlation coefficient between the perinuclear fluorescence signal of the x-axis indicated proteins with respect to TGN46-mRFP (empty circles) or ST-mCherry (gray circles), measured from confocal micrographs in **(B)**. Results are from at least 10 cells from each of n=3 independent experiments (individual values shown, with mean ± stdev). **(D)** HeLa cells co-expressing the different indicated proteins (green and magenta channels) were fixed, processed for immunostaining when required, and the localization of those proteins was monitored by fluorescence confocal microscopy. Insets correspond to zoom-in areas of the dashed, white boxed areas. **(E)** Pearson's correlation coefficient between the perinuclear fluorescence signal of the x-axis-indicated proteins with respect to TGN46-mRFP (empty circles) or VSVG-HA (gray circles; detected by immunofluorescence using an Alexa Fluor 647-conjugated secondary antibody), measured from confocal micrographs in **(D)**. Results are from at least 10 cells from each of n=3 independent experiments (individual values shown, with mean ± stdev). Scale bars in **(B, D)** are 10 µm.

A

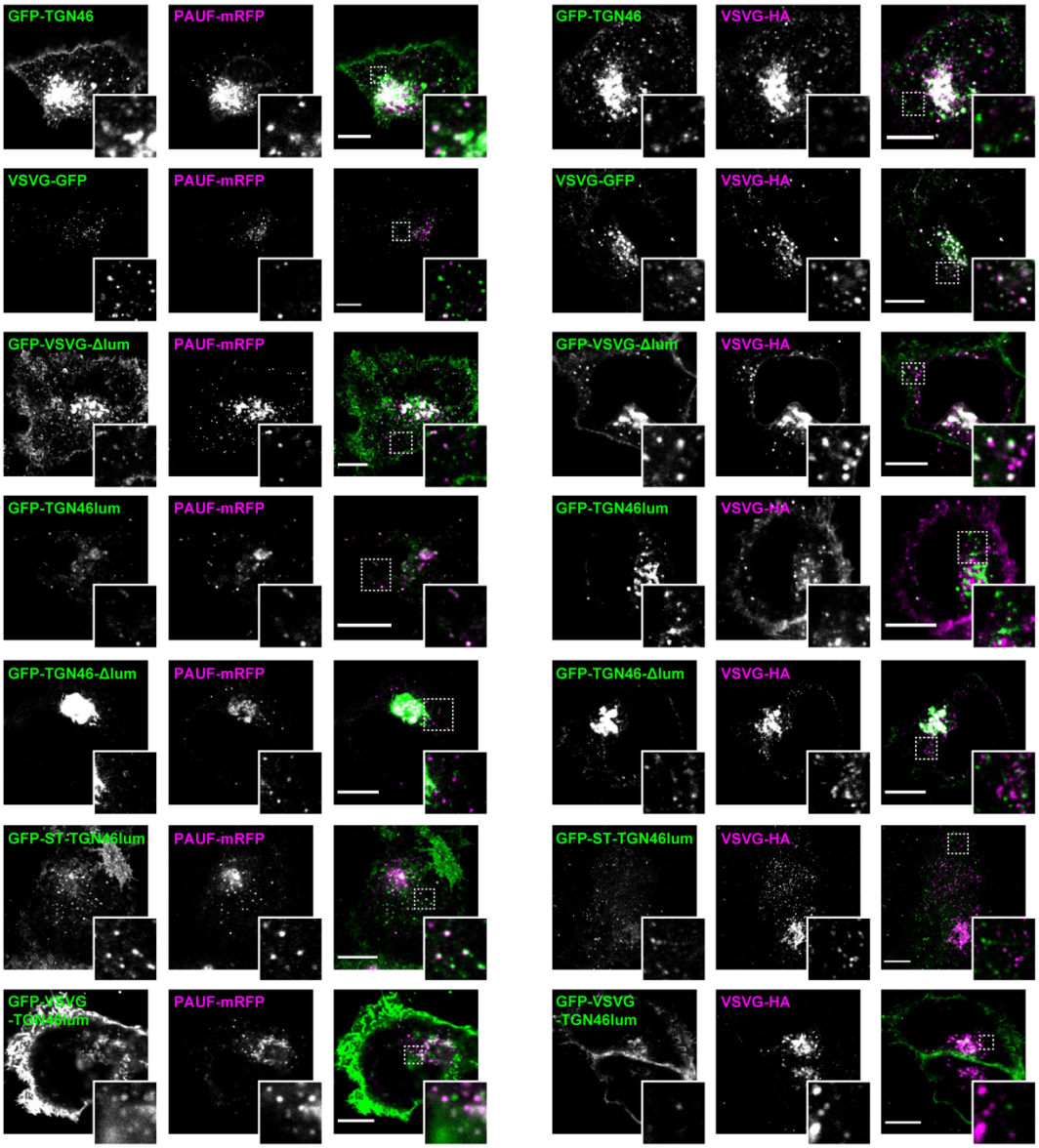
GFP-TGN46
PAUF-mRFP
GFP-TGN46
VSVG-HA
VSVG-GFP
PAUF-mRFP
VSVG-GFP
VSVG-HA
GFP-VSVG-Δlum
PAUF-mRFP
GFP-VSVG-Δlum
VSVG-HA
GFP-TGN46lum
PAUF-mRFP
GFP-TGN46lum
VSVG-HA
GFP-TGN46-Δlum
PAUF-mRFP
GFP-TGN46-Δlum
VSVG-HA
GFP-ST-TGN46lum
PAUF-mRFP
GFP-ST-TGN46lum
VSVG-HA
GFP-VSVG
-TGN46lum
PAUF-mRFP
GFP-VSVG
-TGN46lum
VSVG-HA

B

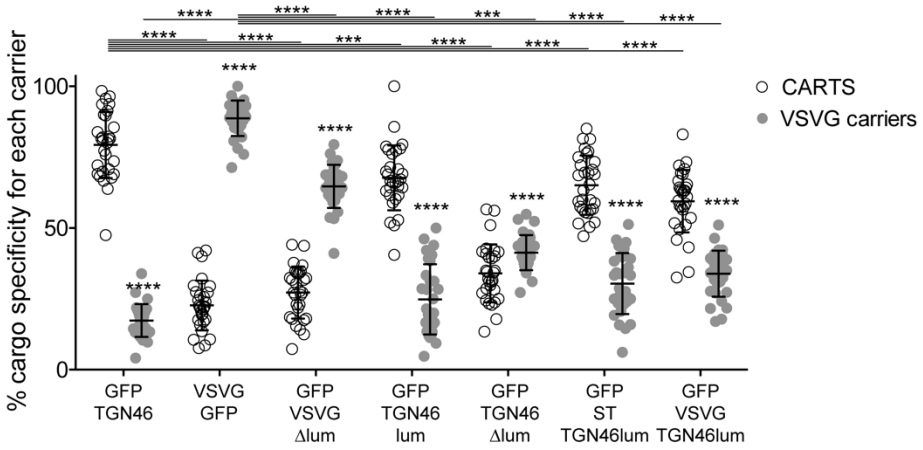
% cargo specificity for each carrier
100
50
0
CARTS
VSVG carriers
GFP TGN46
VSVG GFP
GFP VSVG Δlum
GFP TGN46 lum
GFP TGN46 Δlum
GFP ST TGN46lum
GFP VSVG TGN46lum
****
***

Figure 6. The lumenal domain of TGN46 is necessary and sufficient for its CARTS-mediated export from the TGN. **(A)** HeLa cells co-expressing the different indicated proteins (green and magenta channels) were fixed, processed for immunostaining when required, and the localization of those proteins was monitored by fluorescence confocal microscopy. Insets correspond to zoom-in areas of the dashed, white boxed areas. Scale bars are 10 µm. **(B)** Percentage of transport carriers containing each of the cargoes described on the x-axis that are also positive for PAUF (CARTS, empty circles) or VSVG (VSVG carriers, gray circles), as measured from confocal micrographs in **(A)**. Results are from at least 10 cells from each of n=3 independent experiments (individual values shown, with mean ± stdev).

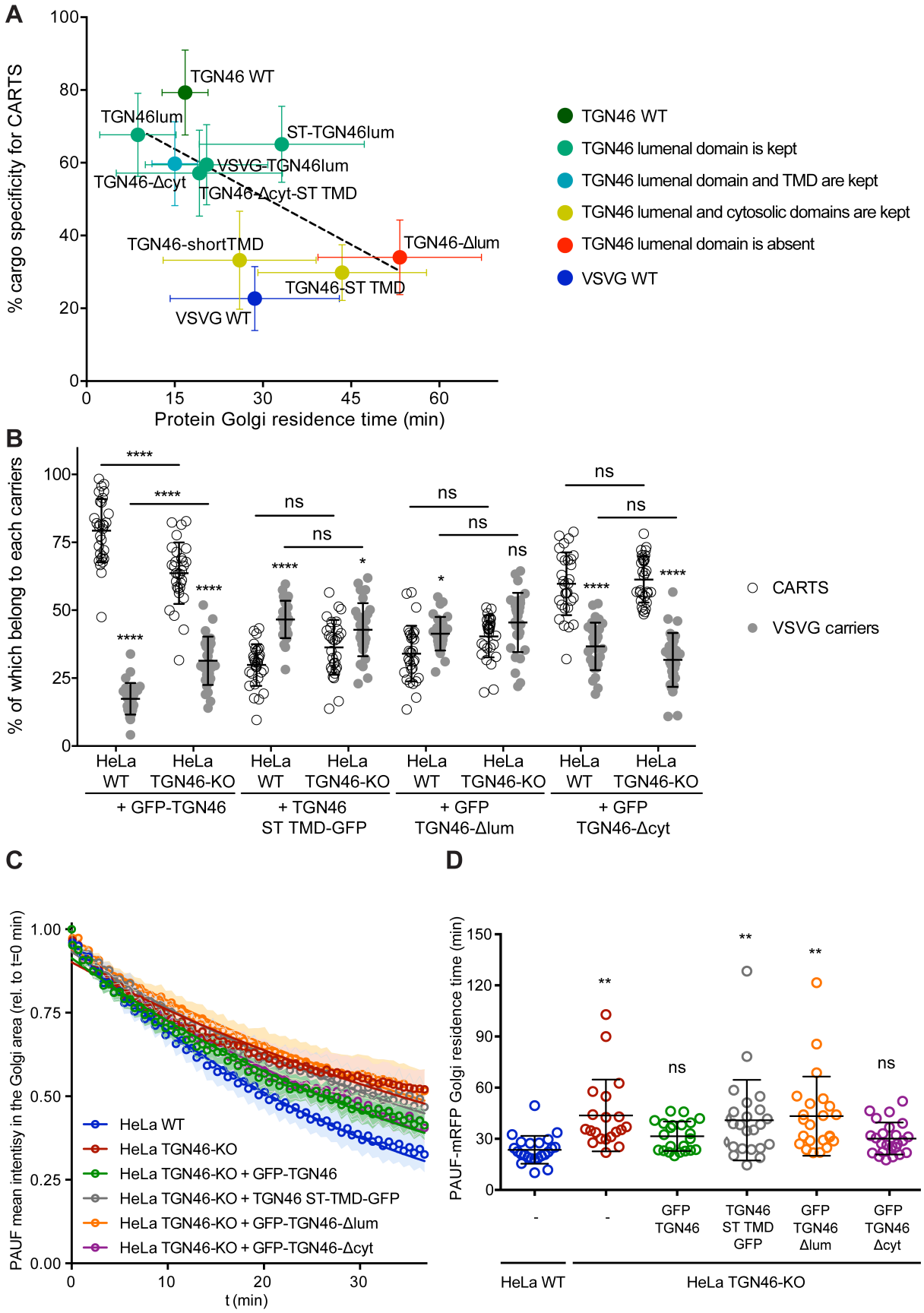

Figure 7. The cargo sorting function of TGN46 is mediated by its lumenal domain. (A) CARTS specificity of cargo proteins correlates with their Golgi export rate. Plot of the percentage of cargo-positive vesicles that are also positive for PAUF (CARTS marker) as a function of the Golgi residence time as measured from FLIP experiments, for the different indicated

cargo proteins (color coding explained in the legend on the right). Dashed black line represents a linear fit of the data points (shown as mean ± s.e.m.), where the slope is statistically different from zero (extra sum-of-squares F test, p value= 0.04). **(B)** Percentage of transport carriers containing each of the cargoes described on the x-axis that are also positive for PAUF (CARTS, empty circles) or VSVG (VSVG carriers, gray circles), as measured from confocal micrographs of HeLa cells (either WT or TGN46-KO cell lines) expressing the indicated proteins. Results are at least 10 cells from each of n=3 independent experiment (individual values shown, with mean ± stdev). **(C)** Relative fluorescence intensity average time trace (mean ± s.e.m.) of FLIP experiments for the indicated proteins expressed in HeLa WT or HeLa TGN46-KO cells, as detailed in the legend. Symbols correspond to actual measurements, solid lines to the fitted exponential decays. **(D)** Residence time of PAUF-mRFP in the perinuclear area of HeLa cells (WT or KO), expressing the different proteins as labeled in the x axis, and measured as the half time of the FLIP curves. Results are from 7–12 cells from each of n=3 independent experiments (individual values shown, with mean ± stdev).